Australian Government
Department of Defence
Defence Science and
Technology Organisation

Parametric Adaptive Matched Filter and its Modified Version

Yunhan Dong

Electronic Warfare and Radar Division
Defence Science and Technology Organisation

DSTO-RR-0313

ABSTRACT

The parametric adaptive matched filter (PAMF) for space-time adaptive processing (STAP) has been an interesting research area in the airborne radar data processing community over the last decade. Starting from providing a complete formulation of PAMF, this report assesses the performance of PAMF using simulated data as well as real airborne data collected by the Multi-channel Airborne Radar Measurements (MCARM) system with use of results from the conventional STAP as a benchmark. A modified PAMF approach using both forward and backward predictions is proposed to eliminate the dimensionality loss of the method. Finally the operational counts and computational savings of PAMF are also estimated.

APPROVED FOR PUBLIC RELEASE

Published by

Defence Science and Technology Organisation
PO Box 1500
Edinburgh South Australia 5111

Telephone: (08) 8259 5555
Fax: (08) 8259 6567

© Commonwealth of Australia 2006
AR-013-643
May 2006

APPROVED FOR PUBLIC RELEASE

Parametric Adaptive Matched Filter and its Modified Version

EXECUTIVE SUMMARY

How to quickly process phased array radar data for small target detection is a key issue of air surveillance radar systems. Much research effort, in particular that sponsored by the Air Force Research Laboratory (AFRL), has been put into developing the parametric adaptive matched filter (PAMF) for space-time adaptive processing (STAP) over the last decade. This report traces, examines and evaluates this technique in great detail. The contribution of this report is manyfold. First a full mathematical formulation of PAMF is provided. Previously published papers on this topic often omit details of the mathematics, possibly due to space limitation, making it difficult for readers to follow through. This report provides an independent derivation for the PAMF algorithm. With the details of the mathematics provided, the concept, advantages and shortcomings of the filter should be understood more thoroughly.

Secondly the performance of PAMF is fully assessed by applying the algorithm to three different types of radar data including the data generated using a generic radar model, data generated using high fidelity airborne radar simulation software, RLSTAP and real airborne radar data collected by the Multi-Channel Airborne Radar Measurements (MCARM) system. The results are compared to benchmarks, the results of space-time adaptive processing (STAP).

Other authors, eg, Roman et al (2000) have observed that PAMF is robust in the situation of having reduced sample data support, but the reason remained unexplained. This paper mathematically explains the reason. There is an equivalent covariance matrix for PAMF, whose dimension is much smaller than the covariance matrix for the conventional STAP. The number of the dominant eigenvalues of the equivalent covariance matrix for PAMF is also much smaller than that for the conventional STAP, so that less sample data are required for estimating the equivalent covariance matrix. From the processing point of view PAMF uses both fast-time and slow-time averaging processing in forming the equivalent covariance matrix, whereas the conventional STAP only utilises fast-time averaging.

Another contribution is the estimation of operational counts (ops) for the PAMF algorithm. Computational savings of PAMF in comparison to the conventional STAP is also provided.

Finally a modified PAMF approach is proposed. The existing PAMF approach only uses forward prediction parameters, leading to a dimensionality loss, which in turn reduces the Doppler resolution and coherent processing gain. In the case where the order of the filter is high and the number of pulses in a coherent process interval (CPI) is small, the loss in coherent processing gain and the loss in Doppler resolution could be significant. The proposed PAMF approach uses both forward and backward prediction parameters to eliminate the dimensionality loss.

Based on this study, the PAMF algorithm has two advantages over the conventional STAP algorithm:

- The requirement of operational counts (ops) is reduced. Computational savings, compared to the STAP algorithm, vary from less than 20% for a system with a small number of pulses, a small number of array elements and a large number of range bins, to more than 90% for a system with a large number of pulses, a large number of array elements and a small number of range bins.
- The PAMF algorithm is much more robust than the STAP algorithm in the case where the set of sample data used for generating the covariance matrix is relatively small.

Problems of the PAMF process include

- Because of the dimensionality reduction, the equivalent temporal independent measurements in a CPI are reduced, which in turn reduces the Doppler resolution and coherent processing gain. The proposed PAMF, which uses both forward and backward prediction parameters, solves the dimensionality reduction problem and maintains the Doppler resolution, and processing gain.
- The clutter profile against range bin using the PAMF processing does not seem to follow the pattern of the original clutter profile. Whether this imposes a problem for target detection warrants further investigation.

All simulations have suggested that using a sliding window to sample the covariance matrix to process each range bin does not statistically improve results. Therefore a preferable option is to use a fixed window to sample the covariance matrix and process a block of range bins, which significantly saves computational cost.

Overall the amount of ops required for the PAMF algorithm is still huge considering the time frame available for airborne radars. How to further reduce ops demand in processing phased array data warrants future research.

Author

Yunhan Dong
Electronic Warfare Division

Dr Yunhan Dong received his Bachelor and Master degrees in 1980s in China and his PhD in 1995 at UNSW, Australia, all in electrical engineering. He then worked at UNSW from 1995 to 2000, and Optus Telecommunications Inc from 2000 to 2002. He joined DSTO as a Senior Research Scientist in 2002. His research interests are primarily in radar signal and image processing, and radar backscatter modelling. Dr Dong was a recipient of both Postdoctal Research Fellowships and Research Fellowships from the Australian Research Council

Contents

1. INTRODUCTION 1

2. MATCHED FILTERING PROCESSING 2

3. PARAMETRIC MATCHED FILTER 5
3.1 Determination of Parameters in Parametric Matched Filtering 8

4. PARAMETRIC ADAPTIVE MATCHED FILTER (PAMF) 10

5. PERFORMANCE RESULTS 13
5.1 Generic Radar Model Data 13
5.2 RLSTAP Data 16
5.2.1 Discussions on Detection Test Statistics 22
5.2.2 Minimum Number of Range Samples 23
5.2.3 Selection of Secondary Data 28
5.3 MCARM Data 30
5.4 Conclusions 37

6. ESTIMATION OF OPERATIONAL COUNTS 37

7. PAMF WITH COMBINED FORWARD AND BACKWARD COEFFICIENTS 42

8. SUMMARY 46

9. ACKNOWLEDGEMENT 47

10. REFERENCES 47

Table 1: Parameters used in the generic radar model. 13

Table 2: parameters used in RLSTAP simulation. 16

Table 3: Target parameters used in the RLSTAP simulation. 17

Table 4: MCARM radar parameters 31

Table 5: MCARM platform parameters 31

Table 6: Ops required for the MF process. 38

Table 7: Ops required for the PAMF process. 39

Figure 1: $\mathbf{R}_f$ is formed by summing up sub-block matrices of $\mathbf{R}_u$ using a moving window for the case of $p = 2$ and $M = 6$. Some of the block elements of $\mathbf{R}_u$ are not used in forming $\mathbf{R}_f$. 10

Figure 2 (a): SINR comparison between MF and PMF ($p = 3$). There is a little PMF SINR loss compared to the MF SINR. 14

Figure 2 (b): The SINR loss of PMF due to the dimensionality loss. 14

Figure 3: Snapshots of clutter, jamming, noise and target signals. 15

Figure 4: Performance comparison between Λ_{PMF} and Λ_{MF}. 15

Figure 5: MF and PMF adaptive patterns. 16

Figure 6: The LULC data superposed on the DTE data of the Washington D. C. area. 17

Figure 7 (a): SINR comparison between MF and PAMF. The PAMF SINR, compared to the MF SINR, shows some not significant but noticeable loss in the vicinities of the clutter notch. 19

Figure 7 (b): The SINR loss of PAMF due to the dimensionality loss. 19

Figure 8: Target detection performance comparison between MF DTS and PAMF DTS. 20

Figure 9: Target detection performance comparison between MF DTS and PAMF DTS, plotted as signal level verses range bin. 20

Figure 10: Target detection performance comparison between MF DTS and PAMF DTS, plotted as signal level verses Doppler frequency. 21

Figure 11: Using a higher order parameter filter, $p = 5$, improves the level of target 2 (the middle range target), but at the cost of Doppler resolution reduction in the PAMF processing. 21

Figure 12: MDTS removes spikes in the vicinity of mainlobe clutter Doppler frequency, but leaves a notch at that frequency. 23

Figure 13: MDTS removes spikes in the vicinity of mainlobe clutter Doppler frequency, but leaves a notch at that frequency. 23

Figure 14: Eigenvalues of $\hat{\mathbf{R}}_u$ estimated using range samples of 1001-1600. 24

Figure 15: Eigenvalues of $\hat{\mathbf{R}}_f$, $p=3$ and $p=5$, estimated using range samples of 1001-1600. 25

Figure 16: Target detection results of MF MDTS with (a) 300 consecutive range samples, 1301:1600 and (b) 200 non-consecutive range samples, 1001:3:1600. 26

Figure 17: Target detection results using 50 (1451:3:1600) samples: (a) MF STM process; (b) to (d) PAMF MST process with p equal to 3, 4 and 5, respectively. 27

Figure 18: Target detection using the PAMF MDTS process with 30 non-consecutive samples, 1511:3:160): (a) $p=3$ and (b) $p=5$. 28

Figure 19: Target detection results plotted in signal-level versus range and Doppler using the PAMF ($p=5$) MDTS process with 30 and 50 non-consecutive samples. 29

Figure 20: Target detection results plotted in signal-level versus range using the PAMF MDTS ($p=5$) process with 30 and 50 non-consecutive samples. 30

Figure 21: Clutter profile against range after the $1/R^3$ range effect is compensated. 32

Figure 22: Signal level versus range and Doppler processed by MF MDTS and PAMF MDTS using a fixed window of 200:630 with an exclusion of 289:309. 33

Figure 23: Signal level versus range processed by MF MDTS and PAMF MDTS using a fixed window of 200:630 with an exclusion of 289:309. 33

Figure 24: Signal level versus range and Doppler processed by MF MDTS and PAMF MDTS using a fixed window of 200:630 with an exclusion of 289:309. 34

Figure 25: MF DTS and PAMF DTS processes produce many spikes at the mainlobe clutter Doppler frequency deteriorating the detection performance. 34

Figure 26: Target detection using MF MDTS and PAMF MDTS processes with a fixed window of 200:2:600 (exclusion of 389:309). 35

Figure 27: Target detection using MF MDTS and PAMF MDTS processes with a fixed window of 200:2:300 (exclusion of 289:300). 36

Figure 28: Target detection using MF MDTS and PAMF MDTS processes with a fixed window of 200:2:260. 36

Figure 29:Target detection using the PAMF MDTS process with a sliding window of (a) 50 non-consecutive samples and (b) 30 non-consecutive samples. 37

Figure 30: Ratio of the PAMF ops to the MF ops, as a function of the number of pulses M, the number of antenna channels N and the number of range cells K_{rg}. 41

Figure 31: Ops required for the MF and PAMF processes. 42

Figure 32: Doppler resolution comparison between the PAMF with forward prediction and the PAMF with both backward and forward predictions. The STAP result is also shown as a benchmark. 45

Figure 33: The impact of the dimensionality loss on the Doppler resolution and processing gain fades as the ratio of $(M-p)/M$ increases. Shown is the target detection of target 1 in the RLSTAP dataset with $M=31$ and $p=5$. 46

1. Introduction

In a scenario using phased array radar for detecting moving targets whose signals are embedded in undesired signals including clutter (echoes from the Earth's surface), broadband jamming and thermal noise, space-time adaptive processing (STAP) yields an optimal signal-to-interference-and-noise ratio (SINR). However, there are two critical issues in real-time implementation of STAP in airborne radar systems. First for a range cell under test (CUT), data from a large number of adjacent range cells are required in order to adaptively compute a reliable covariance matrix of undesired signals. The available sample cells are sometimes fewer than the required for accurate estimation of the covariance matrix. This, however, may be solved by assuming the structure of the covariance matrix to be known (Steiner and Gerlach, 1998, Steiner and Gerlach, 2000, Gerlach and Picciolo, 2003, Bresler, 1988). The second and more critical issue is the computational requirement, which in fact becomes a processing bottleneck at current computer speeds. Numerous algorithms, aimed at reducing the dimensionality of the covariance matrix in both the spatial and temporal domains, have been proposed to minimise the computational demand to satisfy the real-time requirement while maintaining the coherent processing gain at or close to the optimum level (reduced dimensionality also requires fewer sample cells) (Wang and Cai, 1994, Ward and Kogon, 2004, Wang et al, 2003).

Much research effort, notably that carried out and sponsored by the Air Force Research Laboratory (AFRL), has been done towards developing and evaluating the performance of the parametric adaptive matched filtering (PAMF) approach in recent years. Many papers have been published on this topic in the last decade (Roman et al, 2000, Michels et al, 2003, Rangaswamy and Michels, 1997, Rangaswamy et al, 1995, Robey et al, 1992, Roman et al, 1997). The advantages of PAMF include a reduced sample requirement in estimating parameters and a reduced computational requirement (Roman et al, 2000).

Building from a mathematical derivation of the PAMF (Sections 2 to 4) that is missing from the literature (space limitation) the contributions of this report are:

a) An assessment of the performance of the PAMF compared to the traditional matched filter (eg, STAP) in Section 5;
b) An explanation of the observed robustness of the PAMF when applied to reduced data samples;
c) Estimations of the computational load of the PAMF approach in Section 6;
d) In Section 7 a modified PAMF approach that eliminates the dimensionality loss of the PAMF to recover the processing gain and Doppler resolution lost by the PAMF.

2. Matched Filtering Processing

The mathematical notation used in this report follows the convention: boldface uppercase and lowercase letters represent matrices and vectors, respectively, superscripts T and H denote transpose and Hermitian transpose, respectively, and $\mathbb{C}$ and $\mathbb{R}$ stand for the complex and real number fields, respectively. For instance, $\mathbf{x} \in \mathbb{C}^{MN\times 1}$ denotes $\mathbf{x}$ to be an MN-element complex-valued column vector, and $\mathbf{A} \in \mathbb{C}^{MN\times MN}$ denotes $\mathbf{A}$ to be an $MN \times MN$-element complex-valued matrix. The symbol $\otimes$ denotes the Kronecker matrix product, and $E\{\cdot\}$ expectation.

Let a snapshot $\{\mathbf{x}(n) | n = 0,1,\cdots,M-1\}$ with $\mathbf{x}(n) \in \mathbb{C}^{N\times 1}$ be the complex valued sequence at the output of a linear equispaced N-element array after demodulation and pulse compression sampling, corresponding to the return from a single range cell over an M-pulse CPI. If undesired signals $\mathbf{x}_u$ are Gaussian distributed, it is well known that the optimal MF weighting vector is (Compton, Jr, 1988 and Ward, 1994),

$$\mathbf{w}_{MF} = \gamma \mathbf{R}_u^{-1}\mathbf{e} \tag{1}$$

where γ is an arbitrary scalar, which without loss of generality, we will let equal 1. $\mathbf{R}_u = E\{\mathbf{x}_u \mathbf{x}_u^H\} \in \mathbb{C}^{MN\times MN}$ is the covariance matrix of undesired signals. The undesired signals $\mathbf{x}_u$ may consist of clutter, thermal noise and possibly noise jamming. The vector $\mathbf{e} \in \mathbb{C}^{MN\times 1}$ is the desired signal spatial-temporal steering vector, whose explicit expression may be written as,

$$\mathbf{e} = \mathbf{e}(f_{td}) \otimes \mathbf{e}(f_{ts}) \tag{2}$$

where f_{td} and f_{ts} are the normalised target Doppler and spatial (azimuth) frequencies, respectively. Vectors $\mathbf{e}(f_{td})$ and $\mathbf{e}(f_{ts})$ are the desired target temporal and spatial steering vectors, respectively, defined by,

$$\mathbf{e}(f_{td}) = \frac{1}{\sqrt{M}}\left[1 \quad \exp(j2\pi f_{td}) \quad \cdots \quad \exp(j2\pi(M-1) f_{td})\right]^T \tag{3}$$

and

$$\mathbf{e}(f_{ts}) = \frac{1}{\sqrt{N}}\left[1 \quad \exp(j2\pi f_{ts}) \quad \cdots \quad \exp(j2\pi(N-1) f_{ts})\right]^T \tag{4}$$

Using block component notation, (2) may be written as,

$$\mathbf{e}(n) = \frac{1}{\sqrt{M}} \exp(j2\pi n f_{td}) \mathbf{e}(f_{ts}) \qquad n = 0,1,\cdots,M-1 \tag{5}$$

The output of the MF processor is the product of the Hermitian transpose of the optimal weighting vector times the data snapshot,

$$y = \mathbf{w}_{MF}^H \mathbf{x} \tag{6}$$

The coherent processing gain of the MF processor approaches the upper limit, $10\log_{10}(MN)$ dB, for deterministic signals whose bearings differ from the jamming bearings, and whose Doppler frequencies differ from the clutter Doppler frequency in the radar look direction.

Given a target signal $\alpha\mathbf{e}$, the SINR is defined as the ratio of the output target power to the output interference and noise power,

$$SINR_{MF} = \frac{|y_t|^2}{|y_u|^2} = \frac{\xi_t |\mathbf{w}_{MF}^H \mathbf{e}|^2}{\mathbf{w}_{MF}^H \mathbf{R}_u \mathbf{w}_{MF}} = \xi_t \mathbf{e}^H \mathbf{R}_u^{-1} \mathbf{e} \tag{7}$$

where $\xi_t = E\{|\alpha|^2\}$.

The response of the weighting vector to the azimuth and Doppler is referred to as the adapted pattern and defined as (Ward, 1994)

$$P_{MF} = |\mathbf{w}_{MF}^H \mathbf{e}(f_{ts}, f_{td})|^2 \tag{8}$$

where $\mathbf{e}(f_{ts}, f_{td})$ is a general steering vector with Doppler frequency f_{td} varying from –0.5 to 0.5, and spatial frequency f_{ts} (cosine of the azimuth) varying from -1 to 1.

For an unknown signal amplitude, a detection test statistic (DTS) for the MF process has been proposed as the ratio of the output power to the power of interference and noise (Robey et al, 1992),

$$\Lambda_{MF} = \frac{|\mathbf{w}_{MF}^H \mathbf{x}|^2}{\mathbf{w}_{MF}^H \mathbf{R}_u \mathbf{w}_{MF}} = \frac{|\mathbf{e}^H \mathbf{R}_u^{-1} \mathbf{x}|^2}{\mathbf{e}^H \mathbf{R}_u^{-1} \mathbf{e}} \tag{9}$$

Comparing (7) and (9) we can seen that the MF DTS is actually the SINR of the signal $\mathbf{x}$. In operations, when Λ_{MF} exceeds a threshold, target presence is declared.

The DTS Λ_{MF} may be expressed in an alternative way by utilising the LDU block decomposition of $\mathbf{R}_u$. Because $\mathbf{R}_u$ is a positive definite and Hermitian matrix, it can be decomposed in the form of $\mathbf{R}_u = \mathbf{ADA}^H$. In this form, $\mathbf{A} \in \mathbb{C}^{MN \times MN}$ is a lower block-triangular matrix with M identity matrices $\mathbf{I}_N$ along its main block diagonal, and $\mathbf{D} \in \mathbb{C}^{MN \times MN}$ is a block-diagonal matrix with matrices $\mathbf{D}(n) \in \mathbb{C}^{N \times N}$, $n = 0,1,\cdots,M-1$ along its main block diagonal. Substituting $\mathbf{R}_u^{-1} = \mathbf{A}^{-H}\mathbf{D}^{-1/2}\mathbf{D}^{-1/2}\mathbf{A}^{-1}$ in (9) results in,

$$\begin{aligned}\Lambda_{MF} &= \frac{|(\mathbf{D}^{-1/2}\mathbf{A}^{-1}\mathbf{e})^H(\mathbf{D}^{-1/2}\mathbf{A}^{-1}\mathbf{x})|^2}{(\mathbf{D}^{-1/2}\mathbf{A}^{-1}\mathbf{e})^H(\mathbf{D}^{-1/2}\mathbf{A}^{-1}\mathbf{e})} = \frac{|(\mathbf{D}^{-1/2}\mathbf{u})^H(\mathbf{D}^{-1/2}\boldsymbol{\varepsilon})|^2}{(\mathbf{D}^{-1/2}\mathbf{u})^H(\mathbf{D}^{-1/2}\mathbf{u})} \\ &= \frac{|\mathbf{s}^H\mathbf{v}|^2}{\mathbf{s}^H\mathbf{s}} = \frac{|\sum_{n=0}^{M-1}\mathbf{s}^H(n)\mathbf{v}(n)|^2}{\sum_{n=0}^{M-1}\mathbf{s}^H(n)\mathbf{s}(n)}\end{aligned} \tag{10}$$

where $\mathbf{u} = \mathbf{A}^{-1}\mathbf{e}$, $\mathbf{s} = \mathbf{D}^{-1/2}\mathbf{u}$, $\boldsymbol{\varepsilon} = \mathbf{A}^{-1}\mathbf{x}$ and $\mathbf{v} = \mathbf{D}^{-1/2}\boldsymbol{\varepsilon}$. Let $\mathbf{A}^{-1}$ be denoted as,

$$\mathbf{A}^{-1} = \begin{bmatrix} \mathbf{I}_N & \mathbf{0} & \cdots & \mathbf{0} \\ \mathbf{A}_1^H(1) & \mathbf{I}_N & \cdots & \mathbf{0} \\ \vdots & \vdots & \ddots & \vdots \\ \mathbf{A}_{M-1}^H(M-1) & \mathbf{A}_{M-1}^H(M-2) & \cdots & \mathbf{I}_N \end{bmatrix} \tag{11}$$

The block elements $\boldsymbol{\varepsilon}(n)$ and $\mathbf{v}(n)$ can be written as,

$$\boldsymbol{\varepsilon}(n) = \mathbf{x}(n) + \sum_{k=1}^{n}\mathbf{A}_n^H(k)\mathbf{x}(n-k) \qquad n = 0,1,\cdots,M-1 \tag{12}$$

$$\mathbf{v}(n) = \mathbf{D}^{-1/2}(n)\boldsymbol{\varepsilon}(n) \qquad n = 0,1,\cdots,M-1 \tag{13}$$

It can be proven that with or without target signal presence, $\mathbf{v}$ has identity covariance matrix. Therefore, $\mathbf{A}^{-1}$ implements block whitening and $\mathbf{D}^{-1/2}$ implements block unity-variance normalisation. After the whitening, vectors in the sequence $\{\boldsymbol{\varepsilon}(n) | n = 0,1,\cdots,M-1\}$ are uncorrelated in pairs and the covariance of $\boldsymbol{\varepsilon}(n)$ is $\mathbf{D}(n)$. After further block unity-variance normalisation, vectors in the sequence $\{\mathbf{v}(n) | n = 0,1,\cdots,M-1\}$ are uncorrelated in pairs and each has identity covariance. In another words, the undesired signal $\mathbf{x}_u$ that originally satisfies the complex normal distribution, with zero mean and covariance $\mathbf{R}_u$, i.e., $\mathbf{x}_u \sim CN(\mathbf{0}, \mathbf{R}_u)$, is now

transformed into $\mathbf{v}$ that satisfies the complex normal distribution, with zero mean and identity covariance, i.e., $\mathbf{v} \sim CN(\mathbf{0}, \mathbf{I})$.

Equation (12) may be viewed as a result of a moving-average (MA) filter in block mode (Roman et al, 2000). The signal $\mathbf{x}(n)$, $n = 0,1,\cdots,M-1$, is estimated by the forward linear prediction using $\mathbf{x}(n-k)$, $k = 1,\cdots,n$, with the parameters $\mathbf{A}_n^H(k)$, $k = 1,\cdots,n$. The prediction error is $\boldsymbol{\varepsilon}(n)$.

3. Parametric Matched Filter

This Section formulates the parametric matched filter (PMF). Roman et al (2000) mention that some simplifications in the MF DTS, Λ_{MF}, lead to the PMF DTS, Λ_{PMF}, to be given below. In fact there is no direct mathematical connections between Λ_{FM} and Λ_{PMF}, that is, we cannot derive Λ_{PMF} from Λ_{MF}, although we may express both Λ_{MF} and Λ_{PMF} in similar forms.

Assume the data sequence $\{\mathbf{x}(n) | n = p, p+1,\cdots,M-1\}$ is estimated using the pth order forward autoregressive (AR) parameters $\mathbf{A}_f^H(k)$, $k = 1,\cdots,p$. In this process the forward linear prediction $\hat{\mathbf{x}}(n)$ for sample $\mathbf{x}(n)$ is a linear combination of $\mathbf{x}(n-k)$, $k = 1,\cdots,p$, as (Marple, Jr, 1987),

$$\hat{\mathbf{x}}(n) = -\sum_{k=1}^{p} \mathbf{A}_f^H(k)\mathbf{x}(n-k) \qquad n = p, p+1,\cdots,M-1 \tag{14}$$

The forward linear prediction residual is,

$$\boldsymbol{\varepsilon}(n) = \mathbf{x}(n) - \hat{\mathbf{x}}(n) = \sum_{k=0}^{p} \mathbf{A}_f^H(k)\mathbf{x}(n-k) \qquad n = p, p+1,\cdots,M-1 \tag{15}$$

where $\mathbf{A}_f^H(0) = \mathbf{I}_N$. The count n of $\boldsymbol{\varepsilon}(n)$ in (15) starts from p, which is not convenient. By shifting the count n of $\boldsymbol{\varepsilon}(n)$ to start from zero, (15) can be rewritten as,

$$\boldsymbol{\varepsilon}(n) = \sum_{k=0}^{p} \mathbf{A}_f^H(k)\mathbf{x}(n-k+p) \qquad n = 0,1,\cdots,M-p-1 \tag{16}$$

Although (16) and (12) use similar symbols, this is adopted to avoid using too many symbols. Note that the subscript f of $\mathbf{A}_f^H(k)$ in (16) simply means the forward

prediction. Unlike in (12), $\mathbf{A}_f^H(k)$ is now independent of n. Also $\mathbf{A}_f^H(k)$ in (16) in general has nothing mathematically to do with $\mathbf{A}_n^H(k)$ in (12). This will become clear after the derivation of $\mathbf{A}_f^H(k)$ is given in the following subsection.

Similarly we may define the steering residual $\mathbf{u} \in \mathbb{C}^{(M-p)N\times 1}$ as,

$$\mathbf{u}(n) = \sum_{k=0}^{p} \mathbf{A}_f^H(k)\mathbf{e}(n-k+p) \qquad n = 0,1,\cdots,M-p-1 \tag{17}$$

It is worth noting that the dimensionality of the pth order $\boldsymbol{\varepsilon}$ and $\mathbf{u}$ is reduced to $\mathbb{C}^{(M-p)N\times 1}$.

Equations (16) and (17) can be written in more compact forms as,

$$\boldsymbol{\varepsilon} = \begin{bmatrix} \boldsymbol{\varepsilon}(0) \\ \boldsymbol{\varepsilon}(1) \\ \vdots \\ \boldsymbol{\varepsilon}(M-p-1) \end{bmatrix} = \mathbf{B}\mathbf{x} \tag{18}$$

$$\mathbf{u} = \begin{bmatrix} \mathbf{u}(0) \\ \mathbf{u}(1) \\ \vdots \\ \mathbf{u}(M-p-1) \end{bmatrix} = \mathbf{B}\mathbf{e} \tag{19}$$

where the block matrix $\mathbf{B} \in \mathbb{C}^{(M-p)N\times MN}$ has the form of

$$\mathbf{B} = \begin{bmatrix} \mathbf{A}_f^H(p) & \mathbf{A}_f^H(p-1) & \cdots & \mathbf{I}_N & \mathbf{0} & \cdots & \mathbf{0} \\ \mathbf{0} & \mathbf{A}_f^H(p) & \mathbf{A}_f^H(p-1) & \cdots & \mathbf{I}_N & \mathbf{0} & \cdots \\ & & \ddots & & & & \\ \mathbf{0} & \cdots & & \mathbf{0} & \mathbf{A}_f^H(p) & \mathbf{A}_f^H(p-1) & \cdots & \mathbf{I}_N \end{bmatrix} \tag{20}$$

Let $\mathbf{R}_\varepsilon(n) = E\{\boldsymbol{\varepsilon}(n)\boldsymbol{\varepsilon}^H(n)\}$ denote the temporal residual covariance matrix which is Hermitian and positive definite. The LDU decomposition of $\mathbf{R}_\varepsilon(n)$ is,

$$\mathbf{R}_\varepsilon(n) = \mathbf{L}_\varepsilon(n)\mathbf{D}_\varepsilon(n)\mathbf{L}_\varepsilon^H(n) \tag{21}$$

where $\mathbf{L}_\varepsilon(n) \in \mathbb{C}^{N\times N}$ is a lower triangular matrix and its main diagonal elements are unity and $\mathbf{D}_\varepsilon(n) \in \mathbb{R}^{N\times N}$ is a diagonal matrix with its all diagonal elements greater than zero. The transfer matrix $\mathbf{T}(n)$ functioning as both the whitening and unity-variance normalisation for $\boldsymbol{\varepsilon}(n)$ is then,

$$\mathbf{T}(n) = \mathbf{D}_\varepsilon^{-1/2}(n)\mathbf{L}_\varepsilon^{-1}(n) \tag{22}$$

Finally the PMF DTS can be defined as,

$$\Lambda_{PMF} = \frac{|\mathbf{s}^H\mathbf{v}|^2}{\mathbf{s}^\mathbf{H}\mathbf{s}} = \frac{|\sum_{n=0}^{M-p-1}\mathbf{s}^H(n)\mathbf{v}(n)|^2}{\sum_{n=0}^{M-p-1}\mathbf{s}^H(n)\mathbf{s}(n)} \tag{23}$$

where $\mathbf{s}(n) = \mathbf{T}(n)\mathbf{u}(n)$ and $\mathbf{v}(n) = \mathbf{T}(n)\boldsymbol{\varepsilon}(n)$. Equation (23) can be expressed in a compact form with the use of input signal $\mathbf{x}$ and steering vector $\mathbf{e}$ as,

$$\Lambda_{PMF} = \frac{|\mathbf{s}^H\mathbf{v}|^2}{\mathbf{s}^\mathbf{H}\mathbf{s}} = \frac{|\mathbf{e}^H\mathbf{C}_p\mathbf{x}|^2}{\mathbf{e}^H\mathbf{C}_p\mathbf{e}} \tag{24}$$

where

$$\mathbf{C}_P = \mathbf{B}^H\mathbf{R}_\varepsilon^{-1}\mathbf{B} \tag{25}$$

$$\mathbf{R}_\varepsilon = \begin{bmatrix} \mathbf{R}_\varepsilon(0) & & & \\ & \mathbf{R}_\varepsilon(1) & & \\ & & \ddots & \\ & & & \mathbf{R}_\varepsilon(M-p-1) \end{bmatrix} \tag{26}$$

Therefore, analogous to STAP, we may define the PMF weighting vector $\mathbf{w}_{PMF} \in \mathbb{C}^{MN\times 1}$ as,

$$\mathbf{w}_{PAMF} = \gamma\mathbf{C}_P\mathbf{e} \tag{27}$$

The corresponding SINR and adaptive pattern, respectively, are,

$$SINR_{PMF} = \frac{\xi_t|\mathbf{w}_{PMF}^H\mathbf{e}|^2}{\mathbf{w}_{PMF}^H\mathbf{R}_u\mathbf{w}_{PMF}} = \frac{\xi_t|\mathbf{e}^H\mathbf{C}_P\mathbf{e}|^2}{\mathbf{e}^H\mathbf{C}_P\mathbf{R}_\mathbf{u}\mathbf{C}_P\mathbf{e}} = \xi_t\mathbf{e}^H\mathbf{C}_P\mathbf{e} \tag{28}$$

and

$$P_{PMF} = |\mathbf{w}_{PMF}^H \mathbf{e}(f_{ts}, f_{td})|^2 \tag{29}$$

Comparing (24) and (9) or (28) and (7), we see that the matrix $\mathbf{C}_P$ in (24) and (28) functions as the matrix $\mathbf{R}_u^{-1}$ in (9) and (7).

3.1 Determination of Parameters in Parametric Matched Filtering

In the previous subsection we have derived for the PMF algorithm all formulae except the filter parameters $\mathbf{A}_f^H(k)$, $k = 1, \cdots, p$. Different methodologies lead to different algorithms for finding the parameters (Marple, Jr, 1987). Here we follow the least squares method, i.e., the covariance method (Marple, Jr, 1987). Roman et al (2000) has reported that in the context of radar signal processing, the least squares method usually outperforms other methods, such as the Strand-Nuttall method. The derivation below is independent work of the author.

The goal of the least squares method is to find parameters $\mathbf{A}_f^H(k)$, $k = 1, \cdots, p$, which produce a minimum squared residual, $\boldsymbol{\varepsilon}^H \boldsymbol{\varepsilon}$. To find the minimum squared residual, we need to solve the simultaneous equations $\frac{\partial}{\partial \mathbf{A}_f^H(k)} \boldsymbol{\varepsilon}^H \boldsymbol{\varepsilon} = 0$, $k = 1, \cdots, p$ (note that $\mathbf{A}_f^H(0) = \mathbf{I}_N$ is constant). The derivative of a scalar function $f(\mathbf{Q}) \in \mathbb{C}^{1\times 1}$ with respect to $\mathbf{Q} \in \mathbb{C}^{m\times n}$ is an $m \times n$ matrix (Van Trees, 2002, p. 1399),

$$\frac{\partial}{\partial \mathbf{Q}} f(\mathbf{Q}) = \begin{bmatrix} \partial f / \partial q_{11} & \cdots & \partial f / \partial q_{1n} \\ & \ddots & \\ \partial f / \partial q_{m1} & & \partial f / \partial q_{mn} \end{bmatrix} \tag{30}$$

where q_{ik}, $i = 1, \cdots, m$, $k = 1, \cdots, n$, is the element of $\mathbf{Q}$. After tedious but straightforward algebra, the equation satisfying $\frac{\partial}{\partial \mathbf{A}_f^H(k)} \boldsymbol{\varepsilon}^H \boldsymbol{\varepsilon} = 0$, $k = 1, \cdots, p$, is,

$$\left[\mathbf{R}_{ff} \;\vdots\; \mathbf{R}_{f1}\right] \begin{bmatrix} \mathbf{A}_f(p) \\ \vdots \\ \mathbf{A}_f(1) \\ \mathbf{I}_N \end{bmatrix} = \mathbf{0} \in \mathbb{C}^{pN \times N} \tag{31}$$

Therefore we find the parameters as,

$$\mathbf{A}_f = \begin{bmatrix} \mathbf{A}_f(p) \\ \vdots \\ \mathbf{A}_f(1) \\ \hline \mathbf{A}_f(0) \end{bmatrix} = \begin{bmatrix} -\mathbf{R}_{ff}^{-1}\mathbf{R}_{f1} \\ \hline \mathbf{I}_N \end{bmatrix} \tag{32}$$

where $\mathbf{R}_{ff} \in \mathbb{C}^{pN \times pN}$ and $\mathbf{R}_{f1} \in \mathbb{C}^{pN \times N}$ are sub-block matrices of $\mathbf{R}_f \in \mathbb{C}^{(p+1)N \times (p+1)N}$ given by,

$$\mathbf{R}_f = \left[\begin{array}{c|c} \mathbf{R}_{ff} & \mathbf{R}_{f1} \\ \hline \mathbf{R}_{10} & \mathbf{R}_{11} \end{array}\right] = E\{\mathbf{X}_f \mathbf{X}_f^H\} \tag{33}$$

$$\mathbf{X}_f = \begin{bmatrix} \mathbf{x}(0) & \mathbf{x}(1) & \cdots & \mathbf{x}(M-p-1) \\ \mathbf{x}(1) & \mathbf{x}(2) & \cdots & \mathbf{x}(M-p) \\ & \ddots & & \\ \mathbf{x}(p) & \mathbf{x}(p+1) & \cdots & \mathbf{x}(M-1) \end{bmatrix} \tag{34}$$

If the covariance matrix $\mathbf{R}_u$ is known, $\mathbf{R}_f$ can be formed by summing up $M-p$ block matrices of $\mathbf{R}_u$ using a moving $(p+1)N \times (p+1)N$ window diagonally from top to bottom, which may be expressed as,

$$\mathbf{R}_f = \sum_{k=0}^{M-p-1} \mathbf{R}_u(k:k+p) \tag{35}$$

where $\mathbf{R}_u(k:k+p) \in \mathbb{C}^{(p+1)N \times (p+1)N}$ is a block sub-matrix of $\mathbf{R}_u$, with $\mathbf{R}_u(k,k) \in \mathbb{C}^{N \times N}$ as its top left block element and $\mathbf{R}_u(k+p,k+p) \in \mathbb{C}^{N \times N}$ as its bottom right block element. Figure 1 depicts a situation where $\mathbf{R}_f$ is formed by adding four sub-block matrices of $\mathbf{R}_u$, corresponding to the case of $p=2$ and $M=6$. It can be seen that the PMF algorithm does not use all block elements in $\mathbf{R}_u$ to form $\mathbf{R}_f$. This may be considered as an information loss since the block element $\mathbf{R}_u(i,k)$ stands for the correlation between data collected by the ith and kth pulses and its neglect means that the correlation is treated as zero.

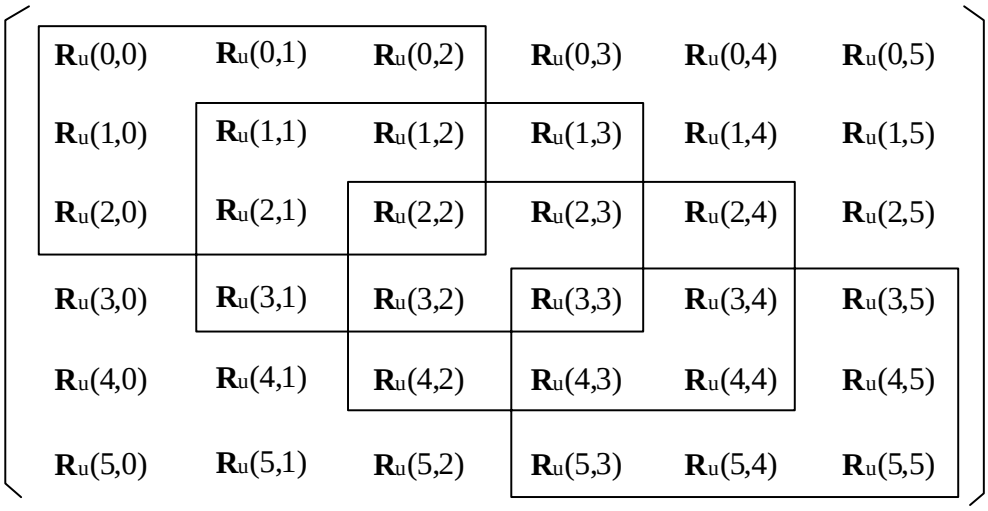

Figure 1: $\mathbf{R}_f$ *is formed by summing up sub-block matrices of* $\mathbf{R}_u$ *using a moving window for the case of* $p = 2$ *and* $M = 6$. *Some of the block elements of* $\mathbf{R}_u$ *are not used in forming* $\mathbf{R}_f$.

4. Parametric Adaptive Matched Filter (PAMF)

In general the covariance matrix of undesired signals $\mathbf{R}_u$ is unknown, so it has to be estimated adaptively using range samples. The often used method is the diagonally-loaded sample matrix (DL-SM) method (Carlson, 1988, Ward and Kogon, 2004), as,

$$\hat{\mathbf{R}}_u = \frac{1}{K}\sum_{k=1}^{K}\mathbf{x}_k\mathbf{x}_k^H + \delta\mathbf{I} \tag{36}$$

where the subscript k denotes range bins. δ is a small value of the order of the system thermal noise level.

The transfer matrix $\mathbf{T}(n)$ $n = 0,1,\cdots,M-p-1$ given by (22) is time-dependent. Roman et al (2000) suggest that a single time-independent transfer matrix $\overline{\mathbf{T}}$ may replace the time-dependent transfer matrix $\mathbf{T}(n)$ in the adaptive process. The time-independent transfer matrix $\overline{\mathbf{T}}$ is obtained through a time-averaging process as,

$$\overline{\mathbf{R}}_{f\varepsilon} = \frac{1}{M-p}\sum_{n=0}^{M-p-1}\mathbf{R}_\varepsilon(n) = \frac{1}{M-p}\mathbf{A}_f^H\mathbf{R}_f\mathbf{A}_f \tag{37}$$

$$\overline{\mathbf{R}}_{f\varepsilon} = \overline{\mathbf{L}}_\varepsilon\overline{\mathbf{D}}_\varepsilon\overline{\mathbf{L}}_\varepsilon^H \tag{38}$$

$$\overline{\mathbf{T}} = \overline{\mathbf{D}}_{\varepsilon}^{-1/2}\overline{\mathbf{L}}_{\varepsilon}^{-1} \tag{39}$$

The PAMF DTS is defined as,

$$\Lambda_{PAMF} = \frac{|\mathbf{s}^H\mathbf{v}|^2}{\mathbf{s}^{\mathbf{H}}\mathbf{s}} = \frac{|\sum_{n=0}^{M-p-1}\mathbf{s}^H(n)\mathbf{v}(n)|^2}{\sum_{n=0}^{M-p-1}\mathbf{s}^H(n)\mathbf{s}(n)} \tag{40}$$

Expressions (40) and (23) are the same, but the difference between Λ_{PMF} and Λ_{PAMF} is that $\mathbf{R}_u$ and $\mathbf{T}(n)$ $n = 0,1,\cdots,M-p-1$, are used for PMF whereas $\hat{\mathbf{R}}_u$ and $\overline{\mathbf{T}}$ are used for PAMF.

Equation (40) can be written in a more compact matrix notation with input signal $\mathbf{x}$ and steering vector $\mathbf{e}$ (Michels et al, 2003). In order to do so, we write,

$$\begin{bmatrix} \mathbf{v}(0) \\ \mathbf{v}(1) \\ \vdots \\ \mathbf{v}(M-p-1) \end{bmatrix} = \begin{bmatrix} \overline{\mathbf{T}} & & \\ & \overline{\mathbf{T}} & \\ & & \ddots \\ & & \overline{\mathbf{T}} \end{bmatrix} \begin{bmatrix} \boldsymbol{\varepsilon}(0) \\ \boldsymbol{\varepsilon}(1) \\ \vdots \\ \boldsymbol{\varepsilon}(M-p-1) \end{bmatrix} \tag{41}$$

This equation can be written as,

$$\mathbf{v} = (\mathbf{I}_{M-p} \otimes \overline{\mathbf{T}})\boldsymbol{\varepsilon} = (\mathbf{I}_{M-p} \otimes \overline{\mathbf{T}})\mathbf{B}\mathbf{x} \tag{42}$$

Similarly,

$$\mathbf{s} = (\mathbf{I}_{M-p} \otimes \overline{\mathbf{T}})\mathbf{u} = (\mathbf{I}_{M-p} \otimes \overline{\mathbf{T}})\mathbf{B}\mathbf{e} \tag{43}$$

Therefore,

$$\mathbf{s}^H\mathbf{v} = \mathbf{e}^{\mathbf{H}}\mathbf{C}_{PA}\mathbf{x} \tag{44}$$

$$\mathbf{s}^H\mathbf{s} = \mathbf{e}^{\mathbf{H}}\mathbf{C}_{PA}\mathbf{e} \tag{45}$$

where

$$\begin{aligned} \mathbf{C}_{PA} &= \mathbf{B}^H(\mathbf{I}_{M-p} \otimes \overline{\mathbf{T}}^H)(\mathbf{I}_{M-p} \otimes \overline{\mathbf{T}})\mathbf{B} \\ &= \mathbf{B}^H(\mathbf{I}_{M-p} \otimes \overline{\mathbf{T}}^H\overline{\mathbf{T}})\mathbf{B} \\ &= \mathbf{B}^H(\mathbf{I}_{M-p} \otimes \overline{\mathbf{R}}_{f\varepsilon}^{-1})\mathbf{B} \end{aligned} \tag{46}$$

Inserting (44) and (45) in (40), we can express the PAMF DTS as,

$$\Lambda_{PAMF} = \frac{|\mathbf{e}^H \mathbf{C}_{PA} \mathbf{x}|^2}{\mathbf{e}^H \mathbf{C}_{PA} \mathbf{e}} \tag{47}$$

Similarly the matrix $\mathbf{C}_{PA}$ in (47) functions as $\mathbf{R}_u^{-1}$ in (9). The PAMF weighting vector $\mathbf{w}_{PAMF} \in \mathbb{C}^{MN}$ defined implicitly in (47) is,

$$\mathbf{w}_{PAMF} = \gamma \mathbf{C}_{PA} \mathbf{e} \tag{48}$$

The SINR for the PAMF is,

$$SINR_{PAMF} = \frac{\xi_t |\mathbf{e}^H \mathbf{C}_{PA} \mathbf{e}|^2}{\mathbf{e}^H \mathbf{C}_{PA} \hat{\mathbf{R}}_{\mathbf{u}} \mathbf{C}_{PA} \mathbf{e}} \tag{49}$$

The adaptive pattern of the PAMF is,

$$P_{PAMF} = |\mathbf{w}_{PAMF}^H \mathbf{e}(f_{ts}, f_{td})|^2 \tag{50}$$

From the above derivation, we may observe some features of the PAMF approach:

- The estimation of the PAMF parameters (coefficients) is achieved by averaging measures not only from a series of range cells collected by the same pulse (Equation (36), fast-time) but also from a series of pulses (Equation (37), slow-time). Hence the estimation procedure is enhanced through the use of both fast-time and slow-time data averaging process.
- It can be seen from Figure 1 that the PAMF does not use the full covariance matrix. In another words, some correlations between data collected by different pulses are treated as zero. This approximation may degrade the performance if the actual correlations are high.
- The original data snapshot consists of a time sequence of M points. Both the PMF and PAMF processes are dimensionality-reduced transformations and contain only a time sequence of $M - p$ points. As we know that the Doppler resolution as well as coherent processing gain is dependent on the length of the time sequence, the reduction in time sequence decreases the Doppler resolution as well as the processing gain. This may not be a concern if $M >> p$. However in the case where the ratio $(M - p)/M$ is low, the loss in the coherent processing gain and the loss in the Doppler resolution may become significant. Section 7 proposes a modified version of PAMF, which does not induce any dimensionality loss.

5. Performance Results

5.1 Generic Radar Model Data

A simple radar model (Ward, 1994) was first used to assess the performance of PMF. Table 1 lists the parameters of the model. The clutter model, which is often referred to as the first-order clutter model, does not take account of temporal and spatial correlation effects (Klemm, 2002) and has the following features,

- Constant clutter coefficient;
- Uncorrelated clutter echoes from patch to patch;
- No range fold-over effect;
- No clutter intrinsic motion.

Table 1: Parameters used in the generic radar model.

Parameter	Specification
Radar	
Phased array	Linear 18-by-4 elements, element pattern $\cos(\phi)$, half-wavelength element spacing, uniform tapering
PRF	300Hz
Number of pulses per CPI	18
Looking direction	Broadside, horizontal
Platform	
Height	9km
Speed	$2v_a/(f_{prf}d)=1$ (DPCA condition), where d is the element spacing
Undesired signals	
Thermal noise	Gaussian
Clutter	First-order clutter model, CNR = 47dB
Jamming	Two equal-intensity broadband jamming signals at azimuth angles of 65^o and 130^o, respectively, JNR = 38dB

Under these assumptions, the covariance matrix $\mathbf{R}_u$ can be formed (Ward, 1994, Dong, 2005). Since $\mathbf{R}_u$ is strictly a Toeplitz-bock-Toeplitz matrix, $\overline{\mathbf{T}}=\mathbf{T}(n)$, $n=0,1,\cdots,M-p-1$. Therefore, there is no discrimination between PMF and PAMF, and the results of PMF and PAMF are the same. Figure 2 (a) shows the SINR comparison between the MF and PMF ($p=3$) processes. The SINR loss of PMF due to

dimensionality loss compared to the MF SINR is shown in Figure 2 (b). The SINR loss due to the dimensionality loss in theory is $10\log_{10}(15/18) = -0.79$ dB.

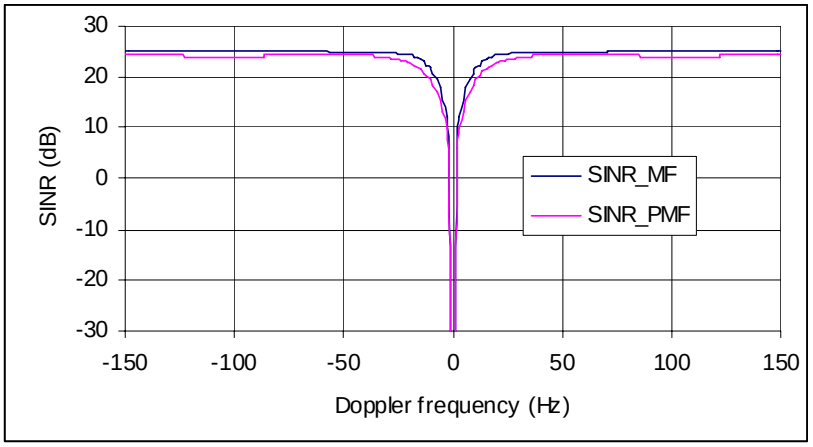

Figure 2 (a): SINR comparison between MF and PMF ($p = 3$). There is a little PMF SINR loss compared to the MF SINR.

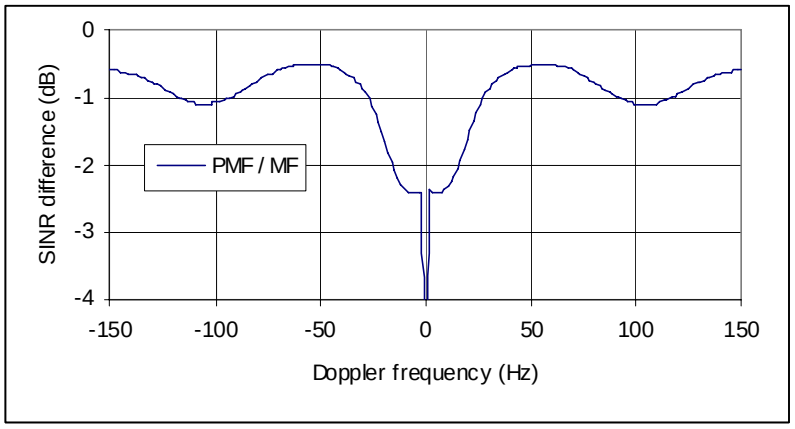

Figure 2 (b): The SINR loss of PMF due to the dimensionality loss.

Assume a target signal $\mathbf{x}_t$ which has a constant amplitude (SNR = 0dB) and constant Doppler (100Hz) is embedded in undesired signals including clutter $\mathbf{x}_c \sim CN(\mathbf{0}, \mathbf{R}_c)$, jamming $\mathbf{x}_j \sim CN(\mathbf{0}, \mathbf{R}_j)$, and thermal noise $\mathbf{x}_n \sim CN(\mathbf{0}, \mathbf{R}_n)$, that is, $\mathbf{x} = \mathbf{x}_t + \mathbf{x}_c + \mathbf{x}_j + \mathbf{x}_n$ and $\mathbf{R}_u = \mathbf{R}_c + \mathbf{R}_j + \mathbf{R}_n$. Figure 3 shows the snapshots of clutter, jamming, thermal noise and target signals. The resultant Λ_{PMF} is compared with

Λ_{MF} in Figure 4. It can be seen from the PAM result that there is a small loss in the peak, and a slight broadening of the mainlobe due to the dimensionality reduction problem as discussed earlier.

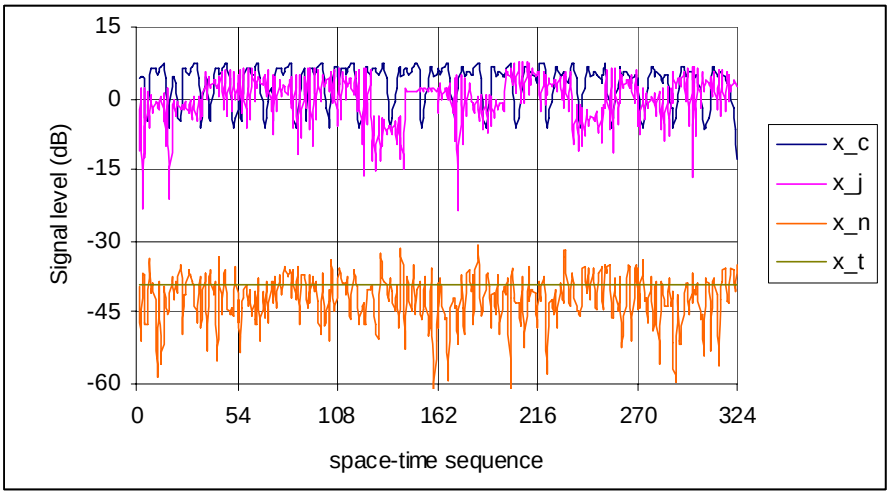

Figure 3: Snapshots of clutter, jamming, noise and target signals.

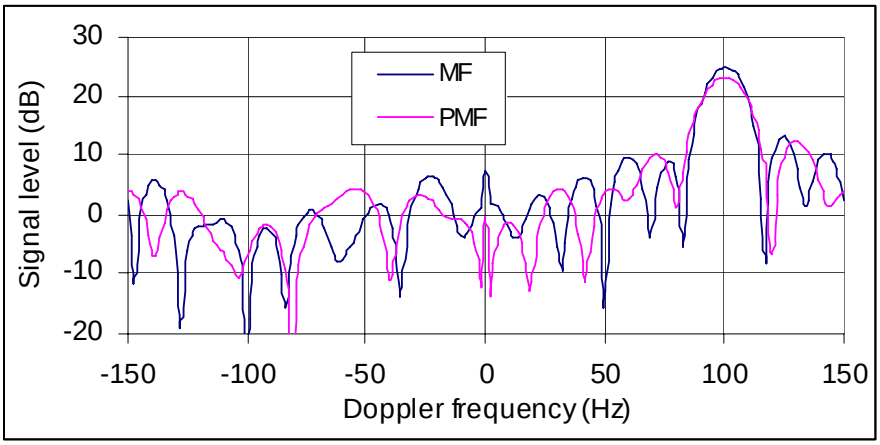

Figure 4: Performance comparison between Λ_{PMF} *and* Λ_{MF} .

Finally the MF and PMF adaptive patterns are shown in Figure 5 assuming a target signal to be at zero azimuth with 100Hz Doppler. The two patterns are very similar.

It can be concluded from the above analysis, for this simulation, that MF and PMF perform approximately the same for this simple radar model.

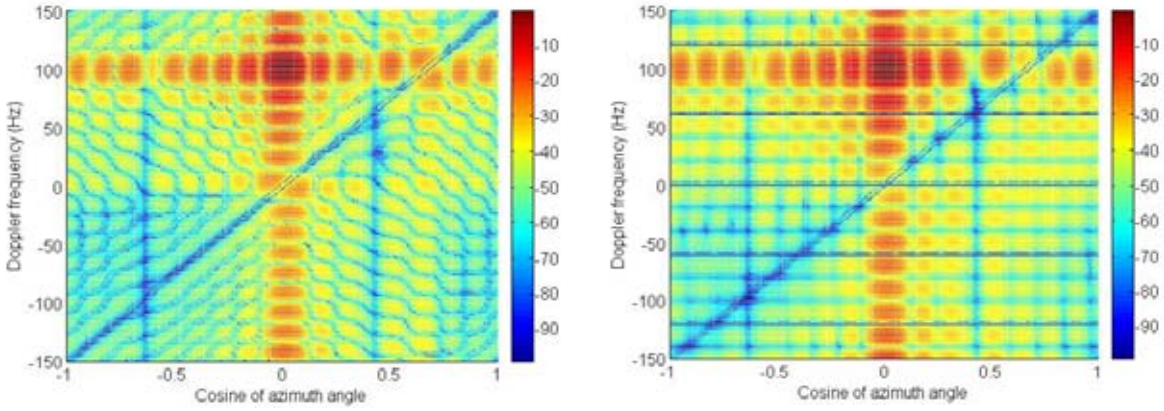

(a) MF (b) PMF, $p = 3$

Figure 5: MF and PMF adaptive patterns.

5.2 RLSTAP Data

The second example used for PAMF evaluation was the data generated by the high fidelity airborne radar simulation software, RLSTAP. Table 2 and Table 3 list radar, platform, environment and target parameters used in the RLSTAP simulation.

Table 2: parameters used in RLSTAP simulation.

Parameter	Specification
Radar	
Phased array	Linear 20-by-4 elements, element pattern $\cos^{0.6}(\phi)$, azimuth spacing 0.12 m, elevation spacing 0.15m uniform tapering for transmit
Carrier frequency	1.2 GHz
Polarisation	VV
LFM bandwidth	2 MHz
PRF	2 kHz
Number of pulses per CPI	32
Peak power	30 kW
Duty	10%
Sample rate	0.2 μs
Looking direction	30^o off the broadside, horizontal
Platform	
Height	7 km
Speed	175 m / s

Undesired signals	
Thermal noise	Gaussian
Clutter	Washington D.C. area
Jamming	None

Table 3: Target parameters used in the RLSTAP simulation.

Parameters	Target 1	Target 2	Target 3
Height (km)	3	3	3
Position off mainlobe direction	1 km north	0.5 km south	0
Radial velocity (m / s)	-100	-20	150
Doppler frequency (Hz)	-500	860	-500
Range (km)	50	60	70
RCS (sqm)	1	1	1

RLSTAP calculates clutter returns based on the United States Geological Survey Land Use and Land Cover (USGS LULC) data and the Digital Terrain Elevation (DTE) data. Details of the clutter calculation model used in RLSTAP are unknown. The clutter environment (Washington D.C. area) seen by the radar is shown in Figure 6.

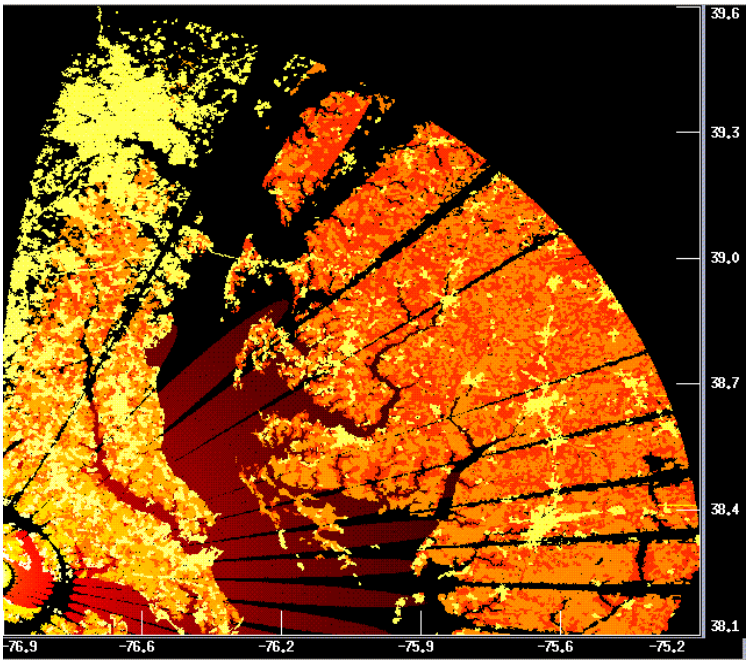

Figure 6: The LULC data superposed on the DTE data of the Washington D. C. area.

The unambiguous range is 75km for the parameters given in Table 2. With the classical $4/3$ Earth radius model, the range to the horizon is 345km resulting in up to four range foldovers. However due to the availability of the LCLU data, the simulation only took the first range foldover into the account. That is, clutter returns from beyond 150km were ignored. Because the clutter return decays as a function of the range to the third power, the effect of higher range foldovers is believed to be insignificant. Accordingly, data collected by the first pulse are discarded in the process, as they do not contain the clutter returns from ambiguous ranges. Therefore the actual number of pulses used in the process was $M = 31$.

To obtain the covariance matrix using the DL-SM method, one might think that the more range samples the better. In fact this is not necessarily true because samples are generally not collected from a statistically homogenous clutter environment. We used four different sampling methods and visually compared the performance of MF for target detection. The ranges bins used in these four cases are,

- Case 1: range bins 800-2650 with the exclusion of target range bins themselves (the target range bins for targets 1, 2 and 3 are 1934, 2266 and 2598, respectively) as well as the 10 nearest range bins on both sides of each target range bin;
- Case 2: range bins 1634-2234 with the exclusion of 1924-1944 (the target range bin is 1934)
- Case 3: range bins 801-1600 (no target in this region);
- Case 4: range bins 1001-1600 (no target in this region).

It has been found that case 1 performed the worst, although it used the most range bins. Cases 3 and 4 performed approximately the same and better than the first two cases. Case 4 was used in the following performance comparison between MF and PAMF.

The SINR comparison between MF and PAMF ($p = 3$) is shown in Figure 7 (a). It is seen that the PAMF SINR shows some noticeable but not significant loss in the clutter notch region in comparison with the MF SINR apart from the loss caused by the dimensionality loss. The SINR loss due to the dimensionality loss in theory is $10\log_{10}(28/31) = -0.44$ dB.

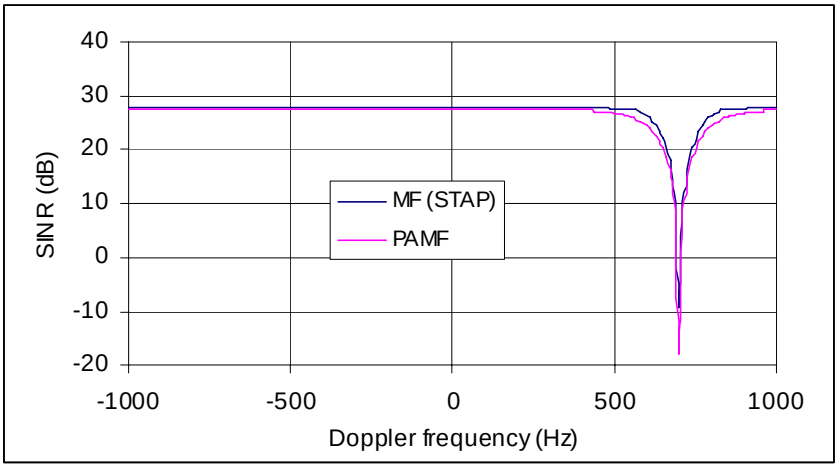

Figure 7 (a): SINR comparison between MF and PAMF. The PAMF SINR, compared to the MF SINR, shows some not significant but noticeable loss in the vicinities of the clutter notch.

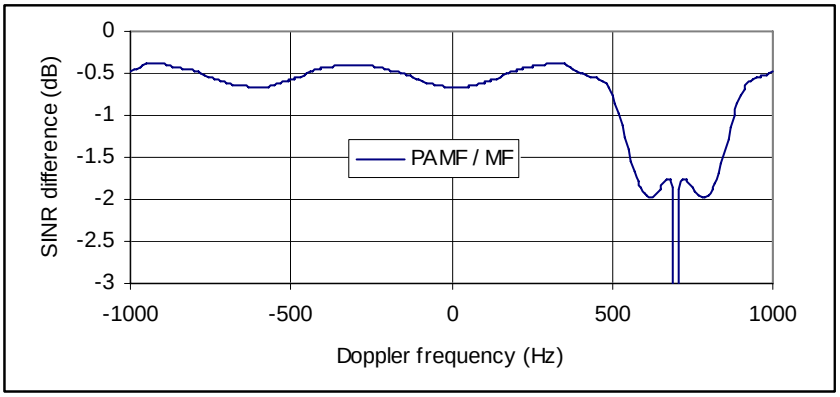

Figure 7 (b): The SINR loss of PAMF due to the dimensionality loss.

Results of MF DTS and PAMF DTS are shown in Figure 8. The performances of the two processors seem approximately the same at first glance. Careful observation, however, indicates that the signal level of target 2 (the target in the middle range bin) in the PAMF process is a few dB lower than the level in the MF process, which is due to the PAMF SINR loss for that frequency as shown in Figure 7. Figure 9 and Figure 10 replot Figure 8 into 2D plots, i.e., signal level versus range and Doppler frequency, respectively. There are only two targets shown in Figure 10, because target 1 (near range) and target 3 (far range) have the same Doppler (refer to Table 3) and are superposed. Figure 9 (a) shows the presence of spikes which could increase the false alarm rate or reduce the detection probability. We will see in due course that these spikes in fact exist in the results of both MF and PAMF DTS processes (though the spikes are much reduced for the PAMF process for this example as shown in Figure 9

(b)) and could become much worse for MCARM data. We discuss what causes these spikes and how to mitigate them in the next subsection.

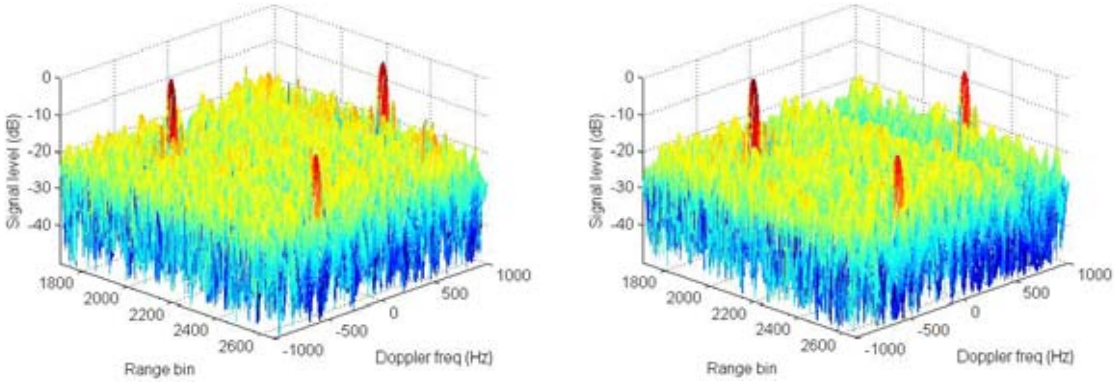

(a) MF (b) PAMF, $p = 3$

Figure 8: Target detection performance comparison between MF DTS and PAMF DTS.

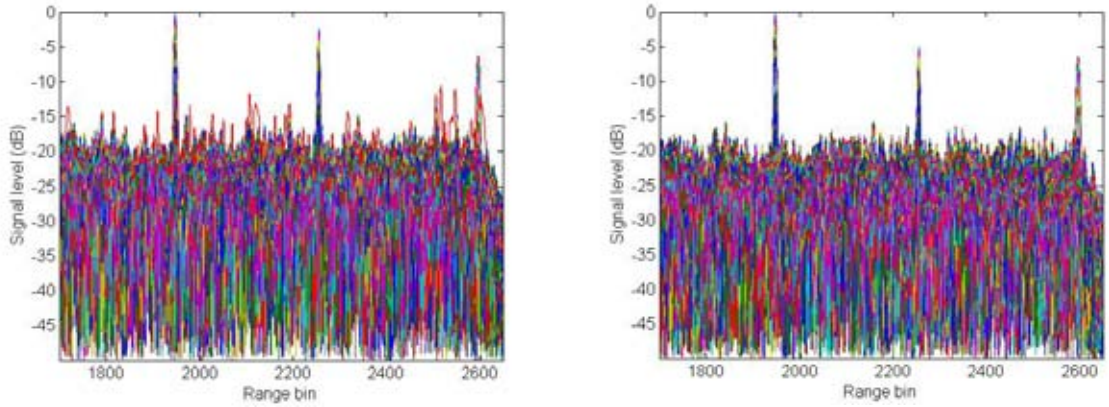

(a) MF (b) PAMF, $p = 3$

Figure 9: Target detection performance comparison between MF DTS and PAMF DTS, plotted as signal level verses range bin.

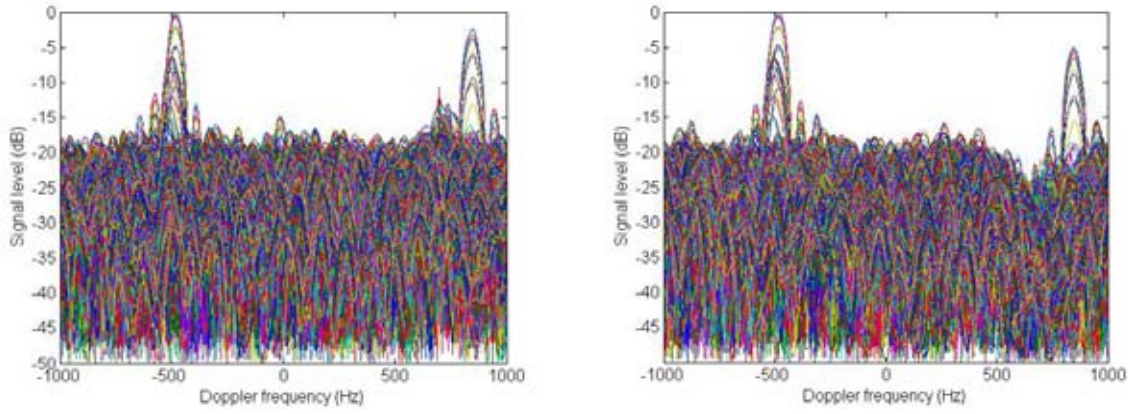

(a) MF (b) PAMF, $p = 3$

Figure 10: Target detection performance comparison between MF DTS and PAMF DTS, plotted as signal level verses Doppler frequency.

If we increase the order of the parameter filter, p, say, from 3 to 5, the SINR loss in the vicinity of the clutter notch for the PAMF is reduced but at the cost of Doppler resolution reduction[1]. Figure 11 shows the detection result of PAMF with $p = 5$ where we can see the signal level of target 2 having been improved compared to the result of $p = 3$ shown in Figure 9 (b).

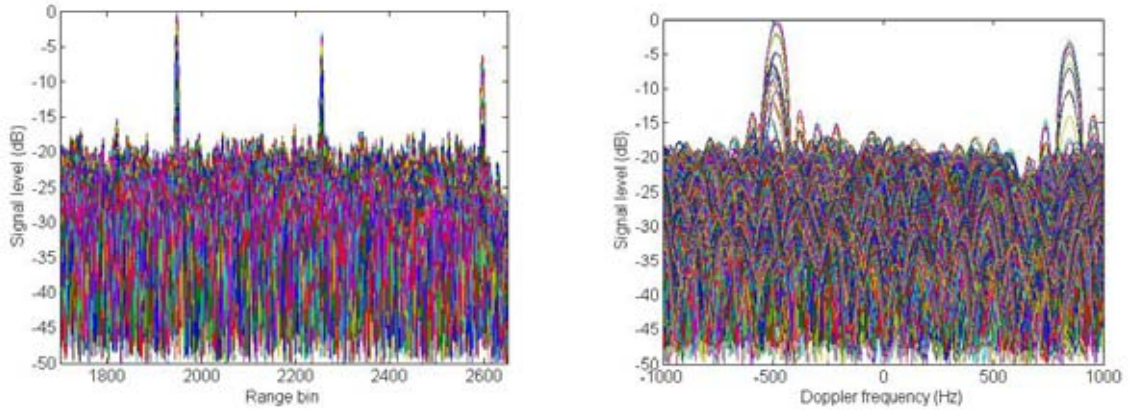

(a) Signal level versus range (b) Signal level versus Doppler

Figure 11: Using a higher order parameter filter, $p = 5$, improves the level of target 2 (the middle range target), but at the cost of Doppler resolution reduction in the PAMF processing.

[1] It means poorer Doppler resolution.

5.2.1 Discussions on Detection Test Statistics

Detection test statistics, Λ_{MF}, Λ_{PMF} and Λ_{PAMF} for MF, PMF, and PAMF, respectively, have been given in (9), (24), and (47), previously. However we have found these test statistics are sensitive to Doppler frequencies of the mainlobe clutter, which may impose a difficulty with target detection and increase the false alarm rate. To explain, let us examine Λ_{MF} from another perspective. When $\xi_t = 1$, (7) can be written as,

$$SINR_{MF}(\xi_t = 1) = \frac{|\mathbf{w}_{MF}^H \mathbf{e}|^2}{\mathbf{w}_{MF}^H \mathbf{R}_u \mathbf{w}_{MF}} = \mathbf{e}^H \mathbf{R}_u^{-1} \mathbf{e} \tag{51}$$

Using the result of (51) we express Λ_{MF} on the decibel scale as,

$$10\log_{10} \Lambda_{MF} = 10\log_{10} |\mathbf{w}_{MF}^H \mathbf{x}|^2 - 10\log_{10} SINR_{MF}(\xi_t = 1) \tag{52}$$

Equation (52) indicates that on the decibel scale Λ_{MF} is the output of the signal minus the SINR of the processor. In general, the SINR of the processor is a constant everywhere except in the frequency vicinity of the mainlobe clutter, where a deep notch is placed (for instance, see Figure 7). Therefore Λ_{MF} on the decibel scale is the output of the processor plus a frequency-independent constant (small in value) outside of the notch region, or a frequency-dependent variable (large in value) in the notch region. The slope of the notch is steep and varies rapidly with frequency. On the other hand, individual data snapshot $\mathbf{x}$ is a random process whose frequency components in the notch region (i.e. clutter) may vary significantly. Therefore, we can expect that fluctuations of Λ_{MF} in the notch region could occur from range bin to range bin, and impose a difficulty on the use of Λ_{MF} for target detection. In fact our interests in target detection using the MF process are generally outside of the clutter notch region. Therefore, simply using the output of the processor, $10\log_{10} |\mathbf{w}_{MF}^H \mathbf{x}|^2$, as a detection test statistic may provide a better result. In order to discriminate, we refer to this as the modified detection test statistic (MDTS). Similar discussion can be made for the other two detection test statistics, Λ_{PMF} and Λ_{PAMF}.

The detection results shown in Figure 12 and Figure 13 are obtained with the use of MDTS. It can be seen that the spikes disappear while a notch at the clutter Doppler frequency appears.

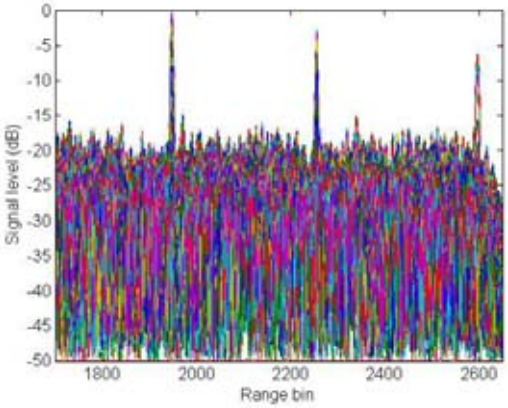

(a) MF MDTS, signal level versus range

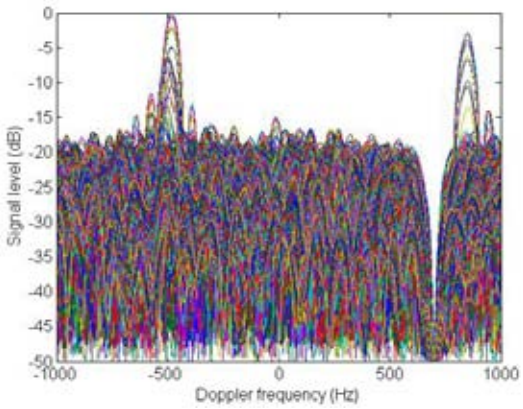

(b) MF MDTS, signal level versus Doppler

Figure 12: MDTS removes spikes in the vicinity of mainlobe clutter Doppler frequency, but leaves a notch at that frequency.

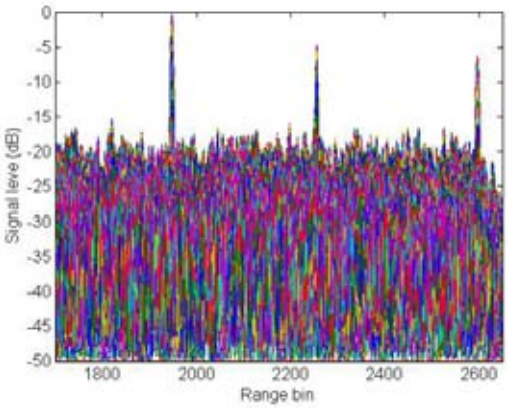

(a) PAMF MDTS, $p = 5$, signal level versus range

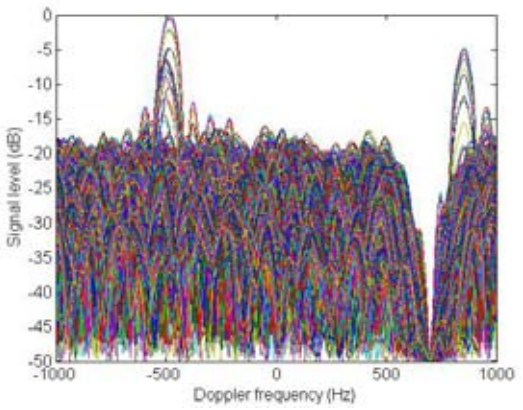

(b) PAMF MDTS, $p = 5$, signal level versus Doppler

Figure 13: MDTS removes spikes in the vicinity of mainlobe clutter Doppler frequency, but leaves a notch at that frequency.

5.2.2 Minimum Number of Range Samples

The unknown covariance matrix of undesired signals is usually estimated using range samples as shown in (33). The conventional question asked is how many range samples are required in order to obtain a reliable estimate of the matrix? Detailed discussions are available in the literature and are out of the scope of this report. Here we only intend to have some discussions from the viewpoint of practical application.

It is well known that given a 3dB tolerance of the optimum performance the number of identically independently distributed (iid) samples needed for estimating a covariance matrix is twice the dimension of the matrix (Reed et al, 1974). However, for the equidistant antenna array and constant PRF, the structure of the covariance matrix has a Toeplitz-block-Toeplitz structure, and the required minimum number of range samples can be greatly reduced (Steiner and Gerlach, 1998, Steiner and Gerlach, 2000, Gerlach and Picciolo, 2003, Bresler, 1998).

In general if we know the eigenvalue distribution of the covariance matrix, we can estimate the minimum number of iid samples required for the covariance matrix. The rank of the covariance matrix of clutter is given by Brennan's rule as (Brennan and Staudaher, 1992, Ward, 1994),

$$N_r = \text{int}\{N + \beta(M-1)\} \tag{53}$$

where $\text{int}\{\cdot\}$ denotes nearest integer; $\beta = 2v_a/(f_{prf}d)$ is the ratio of the normalised Doppler frequency to the normalised spatial frequency, which is also referred to as the number of the clutter fold-overs (Ward, 1994); and d is the azimuth interval of the antenna elements. In fact (53) does not include the effects of the range foldover and clutter intrinsic motion. Therefore, the actual rank of the clutter covariance matrix is normally higher than the theoretical value given in (53), and can be determined by examining the eigenvalues of the sampled covariance matrix. Figure 14 shows the eigenvalues of the covariance matrix $\mathbf{R}_u$ estimated by using range samples 1001-1600. It can be seen that the number of significant eigenvalues in this example is about 170. Analogous to the general rule of two-fold iid samples of the covariance matrix, the number of iid samples required for the covariance matrix in this case is then about $2\times 170 = 340$.

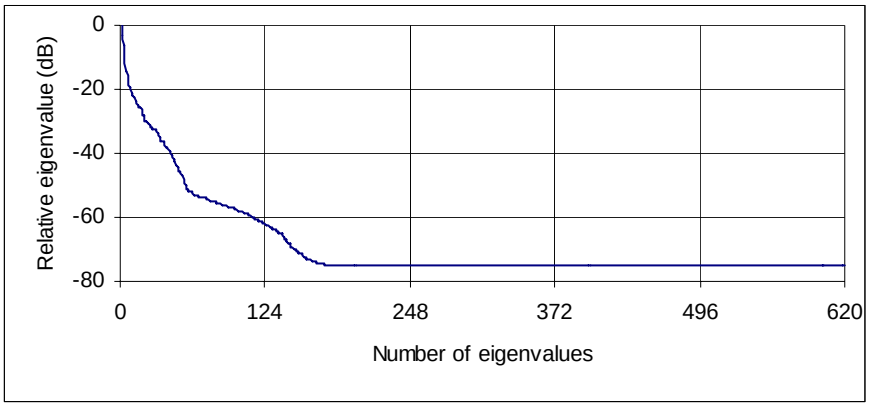

Figure 14: Eigenvalues of $\hat{\mathbf{R}}_u$ estimated using range samples of 1001-1600.

One significant feature of the PAMF, according to Roman et al (2000) is that the method still performs even using a relatively small number of range samples to adaptively estimate parameters. This is because the parameters $\mathbf{A}_f^H(k)$, $k = 0,1,\cdots,M-p-1$, are estimated using $\hat{\mathbf{R}}_f$ rather than $\hat{\mathbf{R}}_u$. The dimension of $\mathbf{R}_f$ is usually much smaller than that of $\mathbf{R}_u$, and so is the number of the dominant eigenvalues. Therefore the number of range samples required for estimating parameters of PAMF can be significantly fewer than the number of samples for estimating the covariance matrix in the conventional MF method. Figure 15 shows the eigenvalue distributions of $\mathbf{R}_f$ with $p=3$ and $p=5$ estimated using range samples 1001-1600. We make two observations from the figure. First, the number of dominant eigenvalues are about the same (26 for $p=3$ and 28 for $p=5$) although the dimension of $\mathbf{R}_f \in \mathbb{C}^{(p+1)N\times(p+1)N}$ varies with p, thus suggesting that using a higher order of p in the PAMF process does not require more iid samples. Second, the number of dominant eigenvalues in $\mathbf{R}_f$ is significantly smaller than that of $\mathbf{R}_u$, so the PAMF method requires far fewer samples in general.

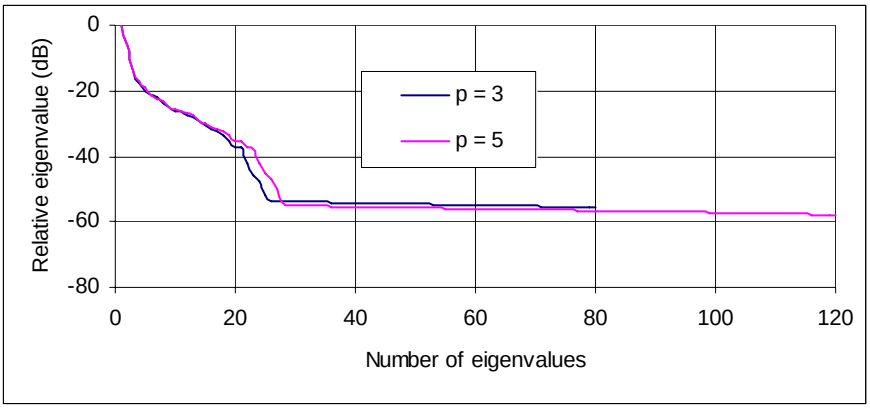

Figure 15: Eigenvalues of $\hat{\mathbf{R}}_f$, $p=3$ and $p=5$, estimated using range samples of 1001-1600.

We notice that the range resolution of the system shown in Table 2 is $\Delta r = c/(2B)$ where c is speed of light and B the bandwidth of the LMF. The corresponding range sampling rate should be $\Delta t = 1/B = 0.5\mu s$. The actual range sampling rate used in RLSTAP was an over-sampled rate of $0.2\mu s$. Therefore, the consecutive range samples may not be iid samples. Shown in Figure 16 are the MF MDTS results with the covariance matrix obtained by averaging (a) 300 consecutive range samples (1301:1600), and (b) 200 non-consecutive range samples with a interval of 3

(1001:3:1600). It can be seen that the detection performance of case (a) is starting to deteriorate, possibly due to only a small portion of the 300 samples being actually iid samples, whereas case (b) performs approximately the same as before, even though the number of samples was reduced to 200. The sampling rate of case (b) is $\Delta t = 3 \times 0.2 \mu s$, and the samples might be considered as iid samples.

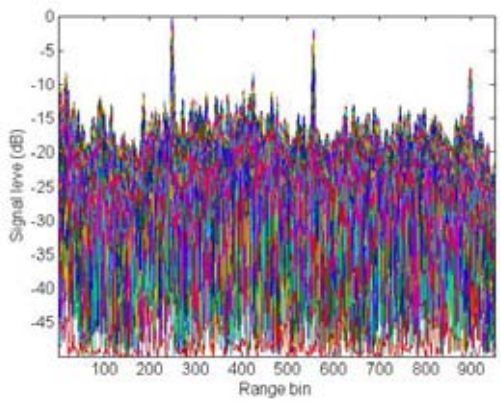

(a) MF MDTS with 300 consecutive range samples

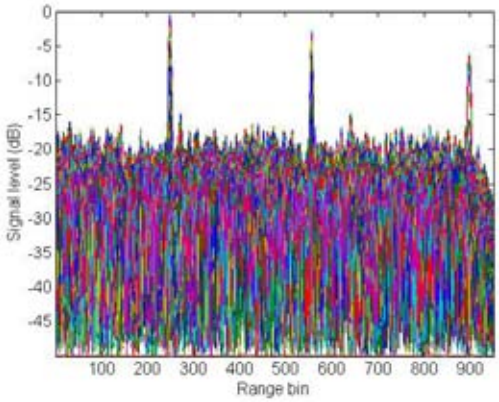

(b) MF MDTS with 200 non-consecutive range samples

Figure 16: Target detection results of MF MDTS with (a) 300 consecutive range samples, 1301:1600 and (b) 200 non-consecutive range samples, 1001:3:1600.

The effect of using fewer samples in the PAMF MDTS is shown in Figure 17 and Figure 18. In particular, the results of Figure 17 and Figure 18 used 50 (1451:3:1600) and 30 (1511:3:1600) samples, respectively. From Figure 17 we see that for this number of samples, the MF process is not functioning, while the PAMF process with $p = 4$ or 5 still maintains a satisfactory level, although the PAMF process with $p = 3$ starts deteriorating. The results of Figure 18 shows that PAMF starts breaking the satisfactory level with $p = 5$, whereas the result of $p = 3$ is unacceptable because of the detection problem on the target in the mid range.

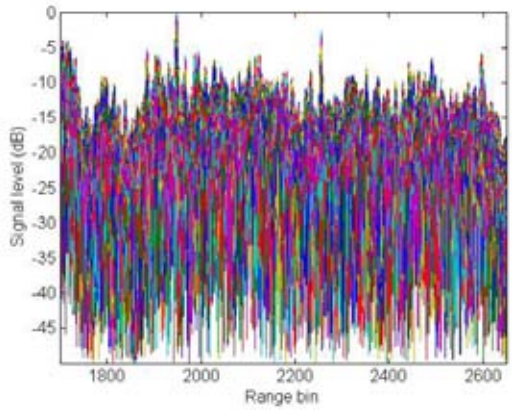

(a) MF MDTS

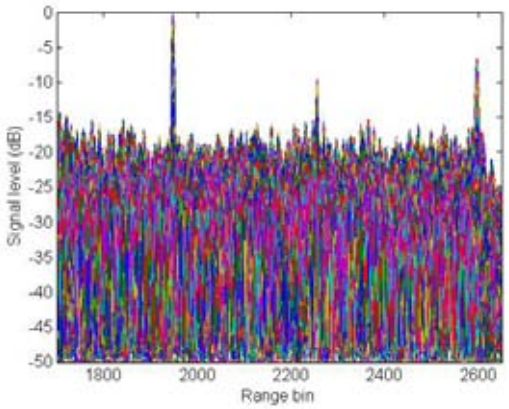

(b) PAMF MDTS, $p = 3$

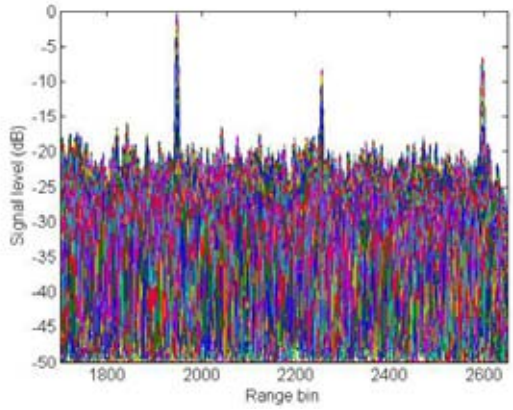

(c) PAMF MDTS, $p = 4$

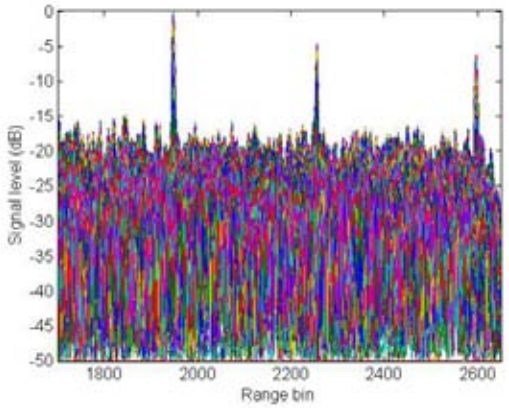

(d) PAMF MDTS, $p = 5$

Figure 17: Target detection results using 50 (1451:3:1600) samples: (a) MF STM process; (b) to (d) PAMF MST process with p equal to 3, 4 and 5, respectively.

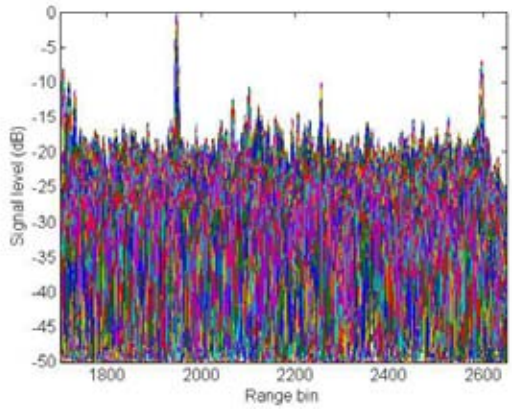

PAMF MDTS, $p=3$

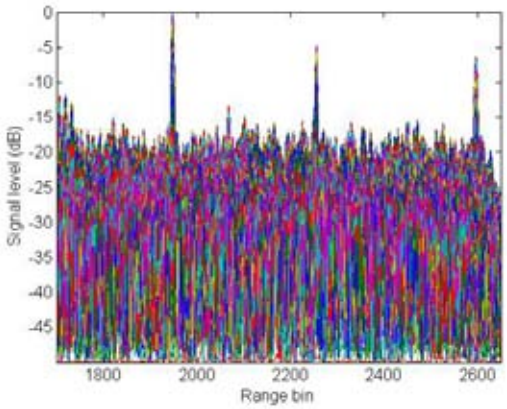

PAMF MDTS, $p=5$

Figure 18: Target detection using the PAMF MDTS process with 30 non-consecutive samples, 1511:3:160): (a) $p=3$ and (b) $p=5$.

5.2.3 Selection of Secondary Data

Data used for sampling $\mathbf{R}_u$ or $\mathbf{R}_f$ are sometimes referred to as secondary data in contrast to primary data which are under test using the statistics of the secondary data. The primary data and secondary data are mutually exclusive. Generally one may use a sliding window or a fixed window to select secondary data (Ward and Kogon, 2004). With the sliding window architecture, the CUT as well as a few guard cells, which normally sit in the centre of the window, are excluded from the sliding window. Since each CUT corresponds to a unique sliding window, it is computationally very expensive. With the fixed window architecture, a single $\hat{\mathbf{R}}_u$ or $\hat{\mathbf{R}}_f$ estimated from a fixed window is used and applied to a block of cells rather than a single cell. All the previous results of RLSTAP data were generated using a fixed window as specified. Theoretically, the sliding window seems to be able to provide better results but has a huge computational cost. However this is not observed in simulation. Figure 19 and Figure 20 compare the PAMF MDST results using a fixed window against a sliding window. The fixed window used was 30 or 50 non-consecutive samples with an interval of 3 (1511:3:1600 or 1451:3:1600). The sliding window also used 30 or 50 non-consecutive samples at an interval of 3, symmetrically on the sides of the CUT plus 5 guard cells at each side. That is, for a CUT k, the sliding window consists of $(k-6-15\times 3:3:k-6)$ and $(k+6:3:k+6+15\times 3)$ or $(k-6-25\times 3:3:k-6)$ and $(k+6:3:k+6+25\times 3)$. We see that little is gained using the sliding window against the fixed window. This is in fact consistent with the findings reported previously (Dong, 2005). The report (Dong, 2005) shows that first the inverse of the covariance matrix is approximately invariant to changes in clutter range cells, and second, the weighting vector is not sensitive to the changes of grazing angle in a certain region.

These two findings explain that a single weighting vector can be applied to a segment of range cells.

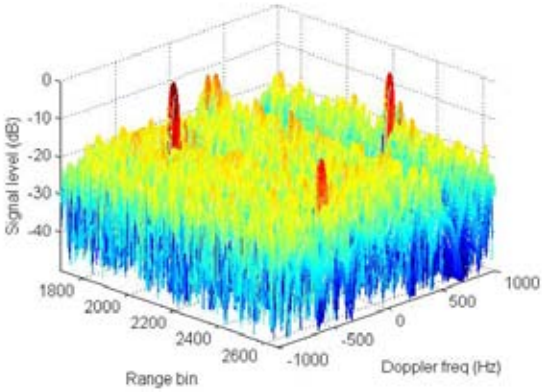

PAMF, $p = 5$, with a fixed window of 30 non-consecutive samples

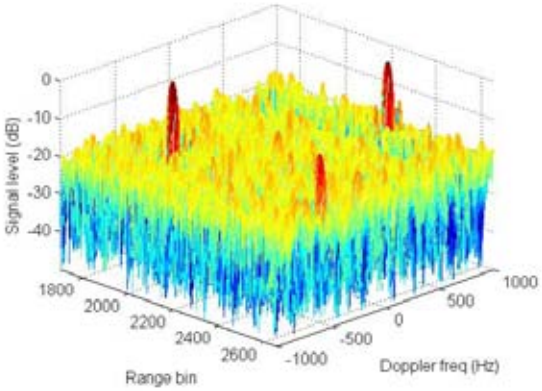

PAMF $p = 5$, with a sliding window of 30 non-consecutive samples

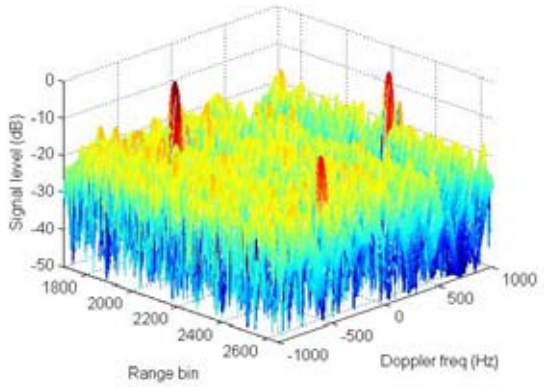

PAMF, $p = 5$, with a fixed window of 50 non-consecutive samples

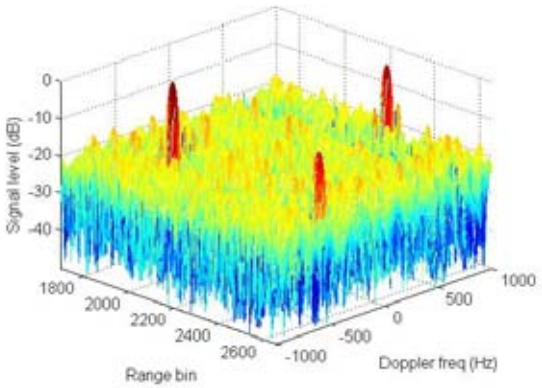

PAMF $p = 5$, with a sliding window of 50 non-consecutive samples

Figure 19: Target detection results plotted in signal-level versus range and Doppler using the PAMF ($p = 5$) MDTS process with 30 and 50 non-consecutive samples.

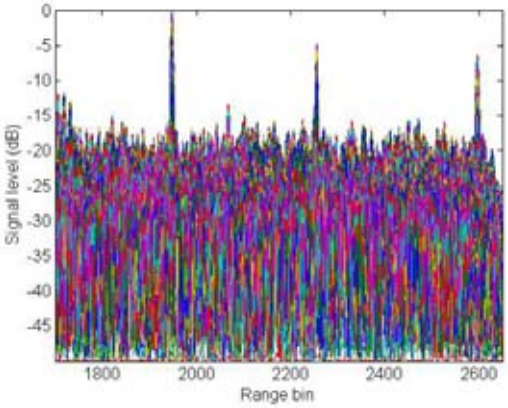

PAMF, $p = 5$, with a fixed window of 30 non-consecutive samples

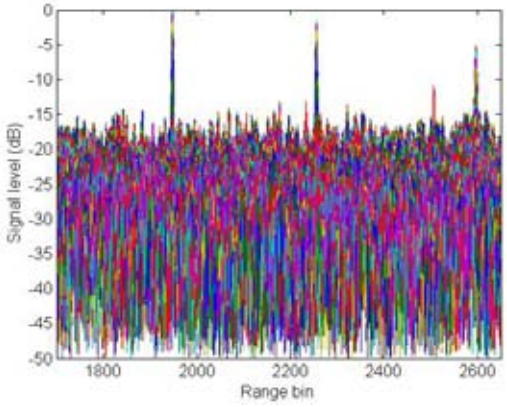

PAMF $p = 5$, with a sliding window of 30 non-consecutive samples

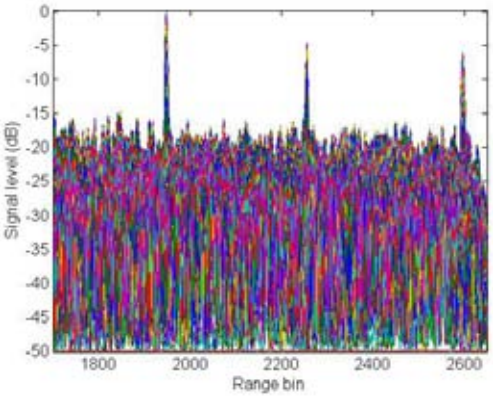

PAMF, $p = 5$, with a fixed window of 50 non-consecutive samples

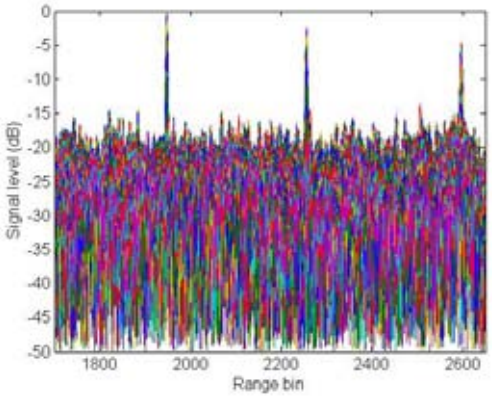

PAMF $p = 5$, with a sliding window of 50 non-consecutive samples

Figure 20: Target detection results plotted in signal-level versus range using the PAMF MDTS ($p = 5$) process with 30 and 50 non-consecutive samples.

5.3 MCARM Data

Detailed descriptions of the multi-channel airborne radar measurement (MCARM) system can be found elsewhere (Sloper etc, 1996, Fenner and Hoover, 1996). Some of the MCARM data analyses are also available (MITRE, 1999, RAFDCI, 1999, Sarker et al, 2001). The dataset #5-575 collected by the MCARM system was used in this report. The radar and platform parameters of #5-575 are given in Table 4 and Table 5, respectively.

Table 4: MCARM radar parameters

Frequency / polarisation	PRF	CPI	Pulse width	Duty	Range resolution	PRI (μs / gates)
1240 MHz / VV	1984	128	50.4 μs	10%	0.8 μs	504 / 630

Table 5: MCARM platform parameters

Height	Velocity	Illumination	Crab angle	Antenna tilt angle from horizontal[2]
3488 m	100.1m / s	Side-looking	7.28^{o}	5.11^{o}

The receiver of the MCARM system consists of 22 receiving channels (modules) in two azimuthal rows. Since these two rows are identical, we treated data received by one row as secondary data and the data received by the other row as primary data. The physical position difference between the two rows will in general induce a phase difference between signal arrivals at the two rows. This however should impose no effect as far as generating the covariance matrix is concerned. We also only used the data collected by the first 50 pulses in the process, hence, $N = 11$ and $M = 50$ in this MCARM data study.

Figure 21 shows the clutter profile of the range bins after compensation for the $1/R^3$ range effect. The area illuminated by the radar mainlobe is mainly farmland with scattered houses (range bins 200-400 and 500-630, for example) and bay water (range bins 400-500, for example). There is a transmitter signal leakage in range bin 68 and the useful clutter data are from around range bin 200 to the end.

[2] This angle is the sum of the antenna tilt angle relative to the platform plus the recorded platform roll angle.

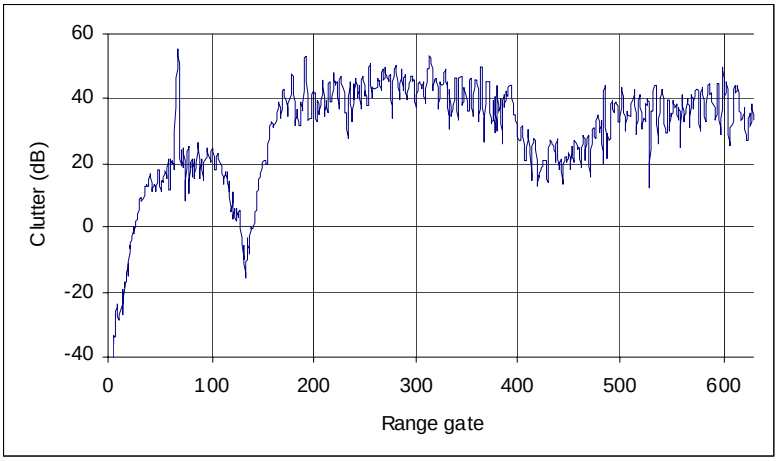

Figure 21: Clutter profile against range after the $1/R^3$ *range effect is compensated.*

A moving target at range bin 299 has been detected and reported previously (Dong, 2005). Range cells 289 to 309 were, therefore, excluded in the secondary data for either the fixed window or sliding window processing.

A fixed window consisting of range cells 200 to 630 but excluding 289 to 309 was first used to sample $\mathbf{R}_u$ for MF processing and $\mathbf{R}_f$ for PAMF processing. The results are shown in Figure 22 to Figure 24. Both processes are able to detect the target at range bin 299. Overall, on average, the noise floor of the MF MDTS result is lower. It is also worth noting that the MF detection profile of signal versus range (Figure 23 (a)) in general follows the clutter profile (Figure 21) whereas the pattern of the PAMF MDTS (Figure 23 (b)) does not show such a feature.

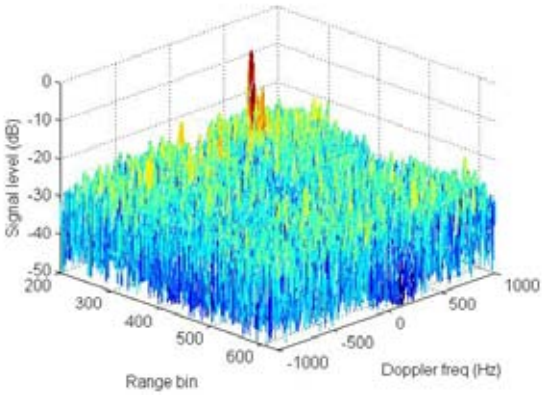

(a) MF MDTS

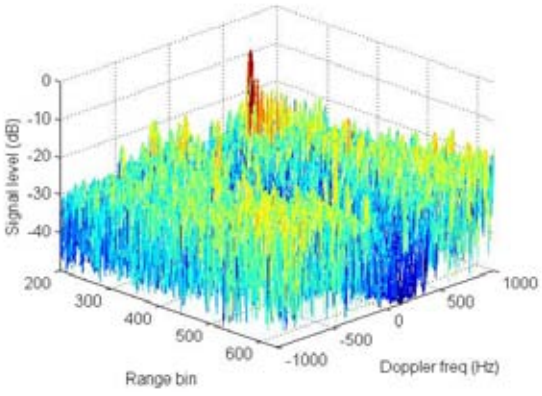

(b) PAMF MDTS, $p = 5$

Figure 22: Signal level versus range and Doppler processed by MF MDTS and PAMF MDTS using a fixed window of 200:630 with an exclusion of 289:309.

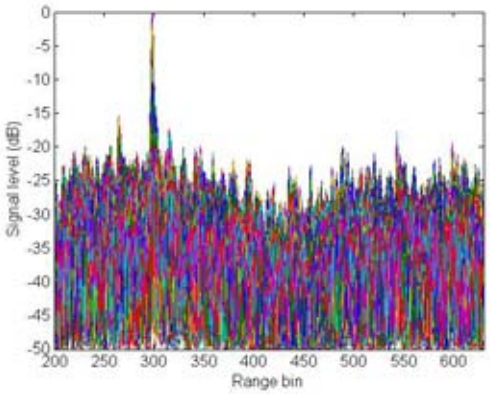

MF MDTS

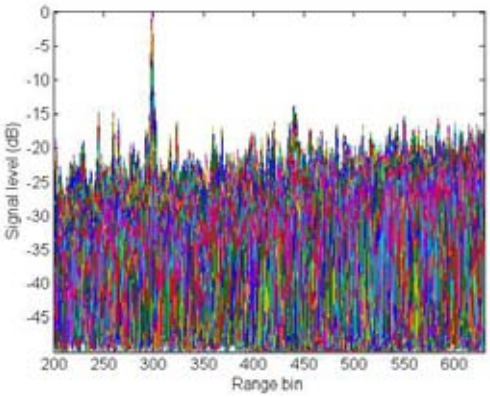

PAMF MDTS, $p = 5$

Figure 23: Signal level versus range processed by MF MDTS and PAMF MDTS using a fixed window of 200:630 with an exclusion of 289:309.

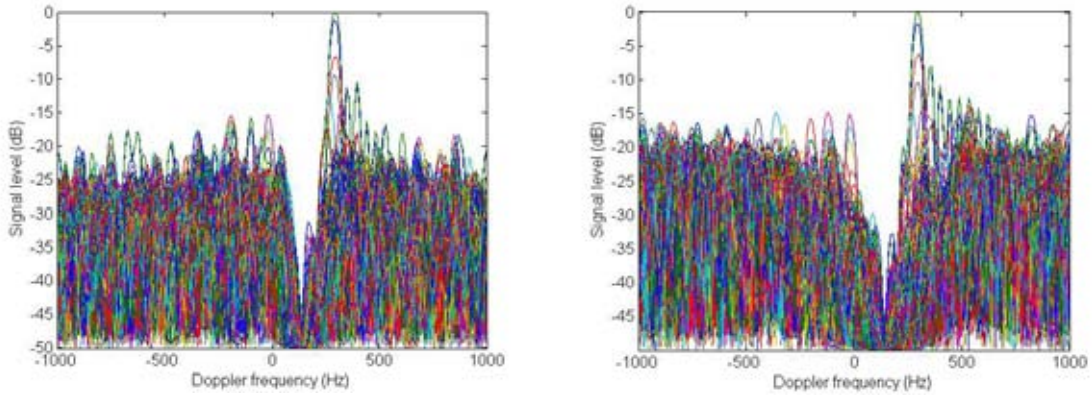

MF MDTS PAMF MDTS, $p = 5$

Figure 24: Signal level versus range and Doppler processed by MF MDTS and PAMF MDTS using a fixed window of 200:630 with an exclusion of 289:309.

The DTS results are shown in Figure 25. We can see from the figure that both MF and PAMF do not sufficiently suppress the clutter, which would significantly increase the false alarm rate should the conventional DTS be used.

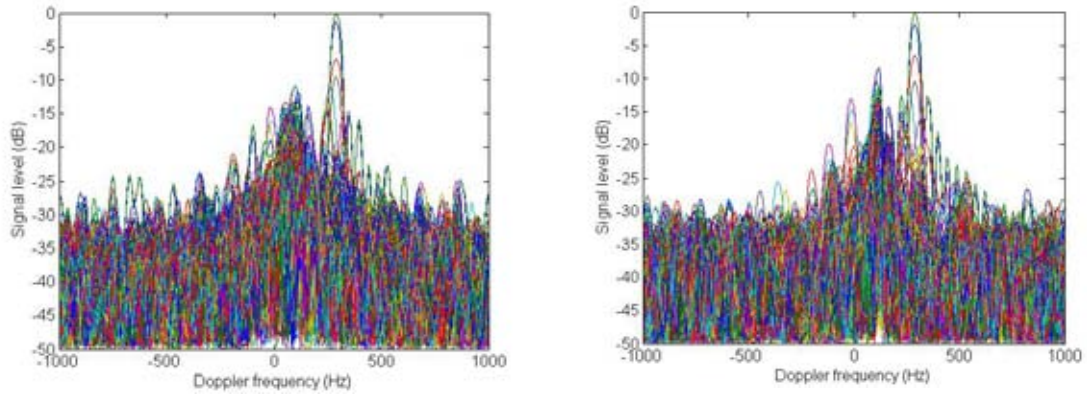

MF MDTS PAMF MDTS, $p = 5$

Figure 25: MF DTS and PAMF DTS processes produce many spikes at the mainlobe clutter Doppler frequency deteriorating the detection performance.

Our next intention is to examine PAMF with reduced secondary data. It is better to use iid samples for such an intention. The consecutive range cells of MCARM data may not be iid samples as the data were also oversampled. The LFM bandwidth of the MCARM system was 1MHz, resulting in that the range sample rate corresponding the range resolution should be $1.0\mu s$ whereas the actual range sample rate was $0.8\mu s$ (see Table

4). Therefore, non-consecutive range samples with an interval of 2 may be considered as iid samples.

Apart from the existing target in range bin 299, we also injected a target signal into range bin 500. The target has a constant amplitude of 30dB below the mean clutter of that bin and a constant Doppler frequency of –200Hz. The results of MF MDTS and PAMF MDTS using three fixed windows, 200:2:600, 200:2:300 and 200:2:260 (excluding the block of 289:309 if applicable) are shown in Figure 26, Figure 27 and Figure 28, respectively. It can be seen that the PAMF process is more robust in terms of using reduced sample data. For the MF process, the injected target, which is detectable with the use of a large number of sample data, becomes non-detectable when the number of samples is reduced. For the PAMF process, on the other hand, the injected target is detectable with all three fixed windows used. The original target in range bin 299 however is always detectable even for the MF process with the window of 200:2:260.

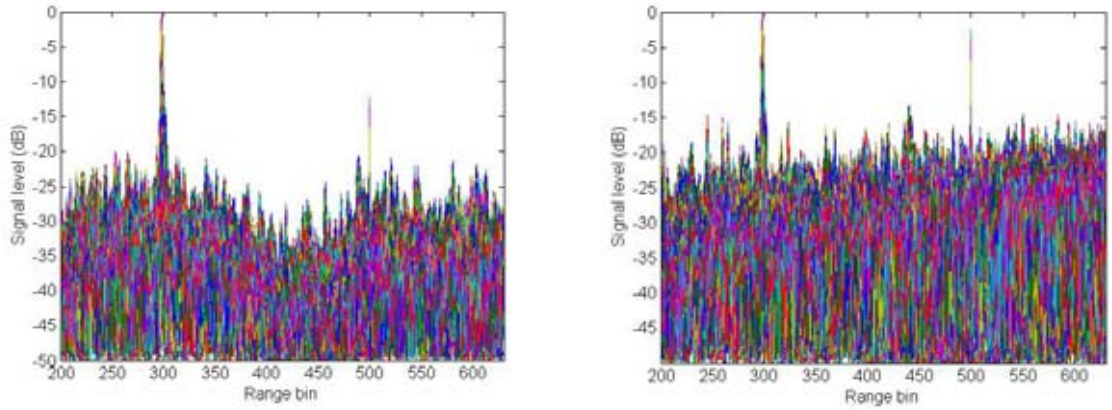

MF MDTS

PAMF MDTS, $p = 5$

Figure 26: Target detection using MF MDTS and PAMF MDTS processes with a fixed window of 200:2:600 (exclusion of 389:309).

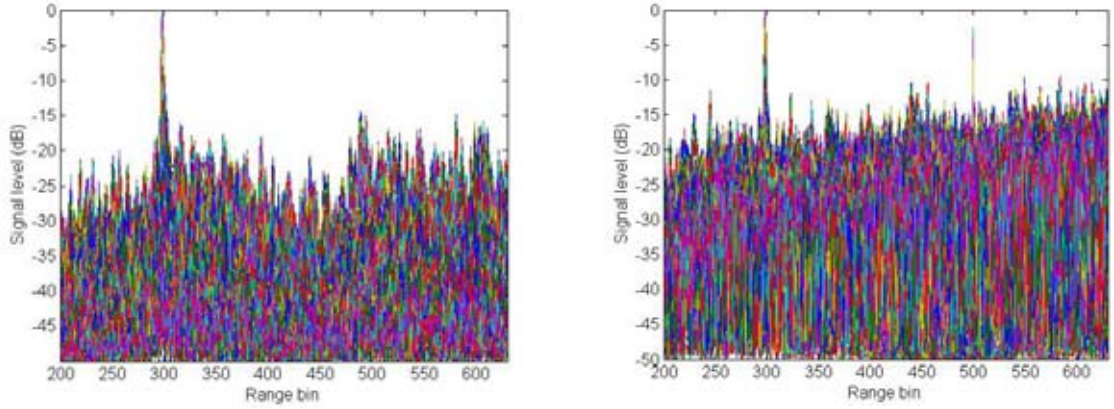

MF MDTS PAMF MDTS, $p = 5$

Figure 27: Target detection using MF MDTS and PAMF MDTS processes with a fixed window of 200:2:300 (exclusion of 289:300).

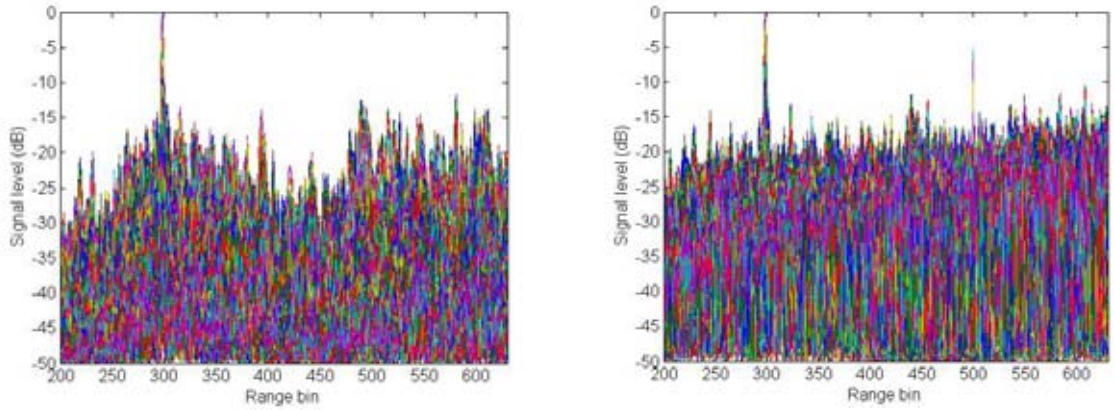

MF MDTS PAMF MDTS, $p = 5$

Figure 28: Target detection using MF MDTS and PAMF MDTS processes with a fixed window of 200:2:260.

Finally the results of PAMF MDTS, with the use of sliding windows of 50 and 30 non-consecutive samples, are shown in Figure 29. It shows again that compared to the results of the fixed windows shown in Figure 27 and Figure 28, there is no improvement in terms of target detection, although a significant amount of additional computation is needed for implementation of the sliding window.

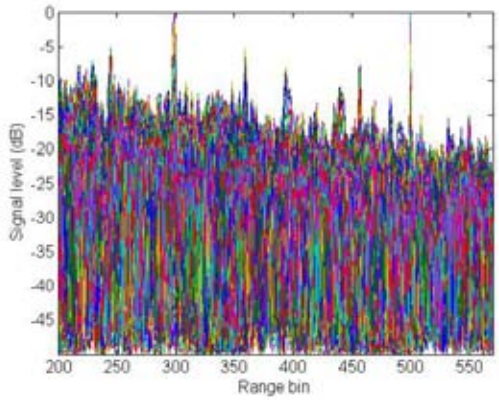

(a) PAMF MDTS, $p = 5$, with a sliding window of 50 non-consecutive samples

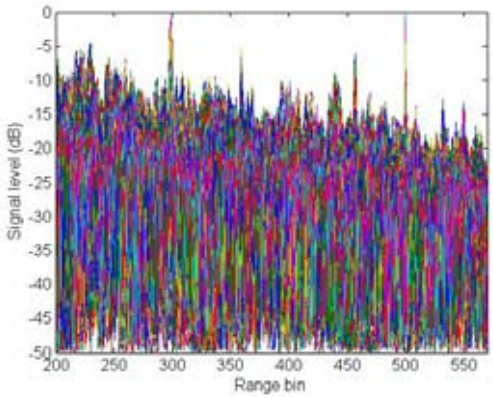

(b) PAMF MDTS, $p = 5$, with a sliding window of 30 non-consecutive samples

Figure 29:Target detection using the PAMF MDTS process with a sliding window of (a) 50 non-consecutive samples and (b) 30 non-consecutive samples.

5.4 Conclusions

The performance of the PAMF approach has been assessed in this Section using three types of radar data. The results of the conventional MF method have served as benchmarks in the assessment. Based on the results, we have observed the following points:

- MF outperforms PAMF if sample data are ample.
- PAMF is much more robust if sample data are limited.
- The sliding window processing does not seem to show a better detection performance, and the fixed window processing is satisfactory and very computationally efficient.
- The conventional DTS by the inclusion of numerically unstable data in the clutter notch can produce false alarms and a modified version (MDTS) generally outperforms the conventional DTS.

Operational counts for the PAMF algorithm and its computational savings compared to the conventional MF algorithm are discussed in the next Section.

6. Estimation of Operational Counts

This section estimates operational counts (ops) for the MF and PAMF algorithms. In the estimation, we only count complex multiplication / division, and ignore addition / subtraction. For simplicity we also assume that no special digital signal

processing (DSP) hardware is used, so that all calculations are treated with the same weight. Special structures of matrices such as complex conjugate, which often lead to special algorithms to save ops, are also not considered. For instance, the number of ops for a matrix multiplication $\mathbf{A}=\mathbf{BC}$ is *lmn* where $\mathbf{A}\in\mathbb{C}^{m\times n}$, $\mathbf{B}\in\mathbb{C}^{m\times l}$ and $\mathbf{C}\in\mathbb{C}^{l\times n}$.

Ops required for the MF and PAMF algorithms are listed in Table 6 and Table 7, respectively.

Table 6: Ops required for the MF process.

Algorithm	Task	Reference Eqn	Ops
$C_{MF}(1)$	$\hat{\mathbf{R}}_u=\sum_{k=1}^{K}\mathbf{x}_k\mathbf{x}_k^H$	(36)	$K(MN)^2$
$C_{MF}(2)$	$\hat{\mathbf{R}}_u^{-1}$	(1)	$(MN)^3$
$C_{MF}(3)$	$\mathbf{w}_{MF}=\hat{\mathbf{R}}_u^{-1}\mathbf{e}$	(1)	$(MN)^2$
$C_{MF}(4)$	$\Lambda_{MF0}=\mathbf{w}_{MF}^H\mathbf{e}$	(9)	MN
$C_{MF}(5)$	$\Lambda_{MF}=\frac{\lvert\mathbf{w}_{MF}^H\mathbf{x}\rvert^2}{\Lambda_{MF0}}$	(9)	MN

Note that the actual ops for $C_{MF}(1)$ may be reduced by a half, if we take account of the Hermitian structure of $\hat{\mathbf{R}}_u$. Similarly, the ops required for $C_{MF}(2)$ may be reduced by a half as $\hat{\mathbf{R}}_u^{-1}$ is also Hermitian. The ops required for the inverse of a matrix are justified by Isaacson and Keller (1966).

Table 7: Ops required for the PAMF process.

Algorithm	Task	Reference Eqn	Ops
$C_{PAMF}(1)$	$\hat{\mathbf{R}}_f$	(35) and (36)	$KN^2[M^2-(M-p)^2+(M-p)]$
$C_{PAMF}(2)$	$\mathbf{A}_f$	(32)	$(pN)^3+p^2N^3$
$C_{PAMF}(3)$	$\overline{\mathbf{T}}$	(37) and (39)	$[(p+1)^2+(p+1)+1]N^3$
$C_{PAMF}(4)$	$\mathbf{u}$	(40)	$pN^2(M-p)$
$C_{PAMF}(5)$	$\mathbf{s}$	(40)	$N^2(M-p)$
$C_{PAMF}(6)$	$\boldsymbol{\varepsilon}$	(40)	$pN^2(M-p)$
$C_{PAMF}(7)$	$\mathbf{v}$	(40)	$N^2(M-p)$
$C_{PAMF}(8)$	$\Lambda_{PAMF0}=\mathbf{s}^H\mathbf{s}$	(40)	$N(M-p)$
$C_{PAMF}(9)$	$\Lambda_{PAMF}=\dfrac{\lvert\mathbf{s}^H\mathbf{v}\rvert^2}{\Lambda_{PAMF0}}$	(40)	$N(M-p)$

In the MF process assuming the Doppler resolution used in Algorithm $C_{MF}(3)$ is $1/(2M)$ (normally the number of Doppler bins is equal to M), we need $2M$ repetitions of $C_{MF}(3)$, $C_{MF}(4)$ and $C_{MF}(5)$ in searching for possible target signals with unknown Doppler frequencies and amplitudes in a single range cell. If we use a fixed window for sampling $\hat{\mathbf{R}}_u$ the total ops for processing a segment of K_{rg} range cells collected by a CPI are,

$$C_{MF}=C_{MF}(1)+C_{MF}(2)+2M[C_{MF}(3)+C_{MF}(4)]+2K_{rg}MC_{MF}(5) \tag{54}$$

Similarly assuming that the Doppler resolution used in calculation for the PAMF processing is $1/(2M)$, and a fixed window is used for sampling $\hat{\mathbf{R}}_f$, then the total ops for processing a segment of K_{rg} range cells collected by a CPI are,

$$\begin{aligned}C_{PAMF}=&C_{PAMF}(1)+C_{PAMF}(2)+C_{PAMF}(3)+2M[C_{PAMF}(4)+C_{PAMF}(5)+C_{PAMF}(8)]+\\&K_{rg}[C_{PAMF}(6)+C_{PAMF}(7)]+2K_{rg}MC_{PAMF}(9)\end{aligned} \tag{55}$$

Shown in Figure 30 is the ratio of the PAMF ops to the MF ops, which is a function of the number of pulses M, the number of antenna channels N and the number of range cells K_{rg}. The other two parameters used in the calculation include $K=50$ and $p=5$.

The fixed window processing is assumed. It can be seen that the computational savings of the PAMF process varies with parameters. For a case where M and N are large, and K_{rg} small, the computational advantage of the PAMF process is significant. On the other hand, if M and N are small, and K_{rg} large, there is not much computational advantage in the PAMF process. This is because when K_{rg} is small, the ops for the inversion of $\hat{\mathbf{R}}_u$ is dominant in the MF processing. However with an increase in K_{rg}, the portion for computing the inverse of $\hat{\mathbf{R}}_u$ in the whole process becomes less dominant.

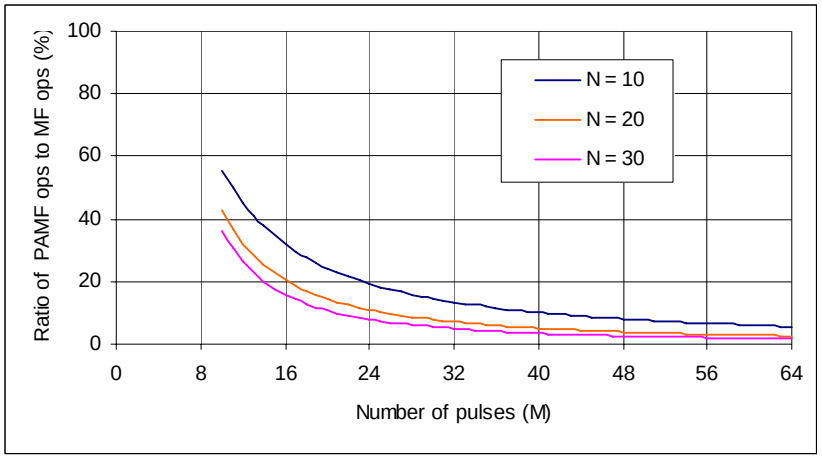

(a) $K_{rg} = 100$

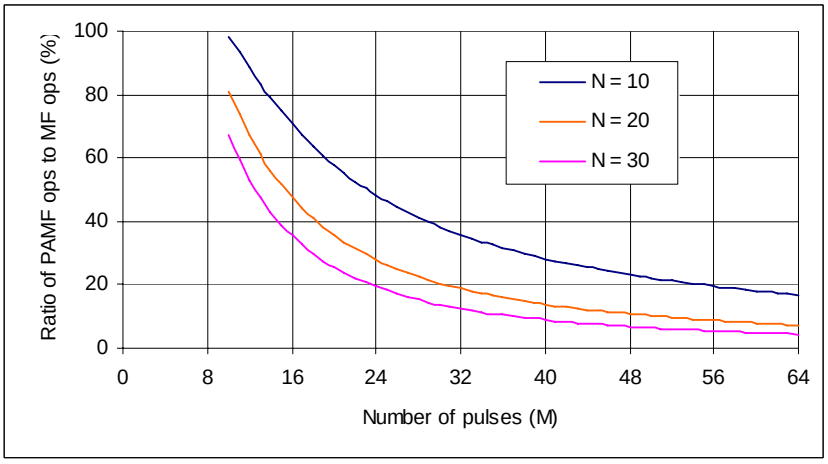

(b) $K_{rg} = 500$

Figure 30: Ratio of the PAMF ops to the MF ops, as a function of the number of pulses M, the number of antenna channels N and the number of range cells K_{rg}.

Ops required by the MF and PAMF processes are shown in Figure 31. It shows the amount of ops even for the PAMF process is still huge, considering the time frame for a CPI to be in a scale of milliseconds for airborne radars. Therefore how to further reduce ops will still be an active research area in the future. The figure also shows that for the same process, an increase in the number of range cells to be processed does not incur a significant increase of ops. Therefore, using a fixed window to process a large chunk of range cells should be a preferable option.

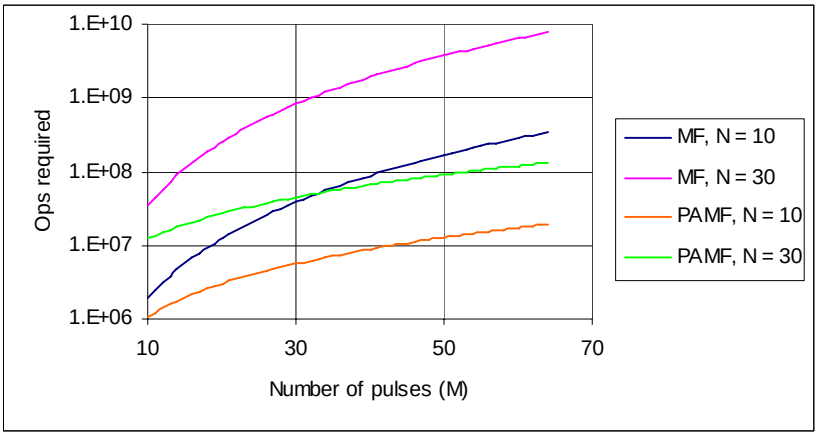

(a) $K_{rg} = 100$

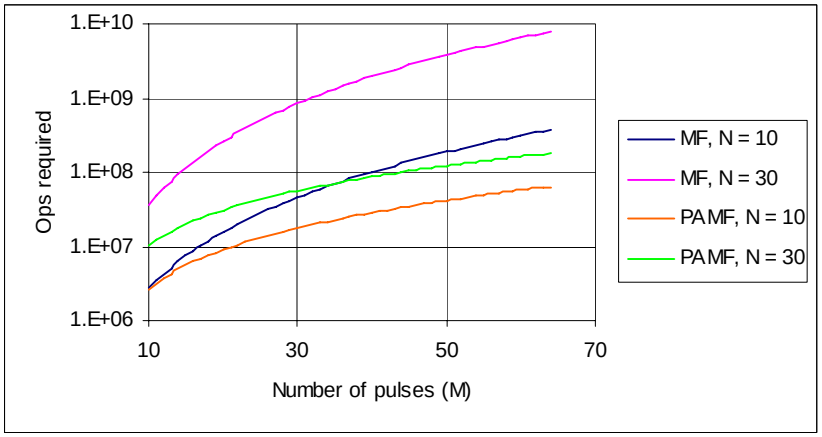

(b) $K_{rg} = 500$

Figure 31: Ops required for the MF and PAMF processes.

7. PAMF with Combined Forward and Backward Coefficients

One of the problems of the PAMF method is the dimensionality loss mentioned in Section 3. Using the pth order AR parameters $\mathbf{A}_f^H(k)$, $k = 1, \cdots, p$, we can only estimate $\{\hat{\mathbf{x}}(n) | n = p, p+1, \cdots, M-1\}$ from the original data sequence $\{\mathbf{x}(n) | n = 0, 1, \cdots, M-1\}$. It means that the original M-point time sequence now becomes an $(M-p)$-point time sequence. As we know that both the Doppler resolution and processing gain are proportional to the number of points in a time

sequence, the dimensionality reduction directly results in a loss in the Doppler resolution and processing gain. The impact can be small or significant depending on the values of M and p. In the case where the ratio of $(M-p)/M$ is small, the impact can be significant.

Equation (14) is a process of the forward linear prediction which estimates the sequence $\{\hat{\mathbf{x}}(n)|n=p, p+1,\cdots,M-1\}$. The sequence $\{\hat{\mathbf{x}}(n)|n=0,1,\cdots,p-1\}$, which cannot be estimated using the forward linear prediction, however, may be estimated with the use of the backward linear prediction as (Marple, Jr, 1987),

$$\hat{\mathbf{x}}(n) = -\sum_{k=1}^{p} \mathbf{A}_b^H(k)\mathbf{x}(n+k) \qquad n=0,1,\cdots,p-1 \tag{56}$$

where $\mathbf{A}_b^H(k)$, $k=1,\cdots,p$, are backward prediction parameters. Together with the forward prediction given in (14), we now have a full dimension of the linear prediction residual as,

$$\boldsymbol{\varepsilon}(n) = \mathbf{x}(n) - \hat{\mathbf{x}}(n) = \begin{cases} \sum_{k=0}^{p} \mathbf{A}_b^H(k)\mathbf{x}(n+k) & n=0,1,\cdots,p-1 \\ \sum_{k=0}^{p} \mathbf{A}_f^H(k)\mathbf{x}(n-k) & n=p, p+1,\cdots,M-1 \end{cases} \tag{57}$$

The remaining process is the same and there is no need to repeat it here except to define the estimates of the backward parameters, $\mathbf{A}_b(k)$, $k=1,\cdots,p$. In order to find these parameters, we need to find the minimum squared residual given by (58),

$$\min\{\boldsymbol{\varepsilon}^H\boldsymbol{\varepsilon}\} = \min\sum_{n=0}^{p-1} \boldsymbol{\varepsilon}^H(n)\boldsymbol{\varepsilon}(n) + \min\sum_{n=p}^{M-1} \boldsymbol{\varepsilon}^H(n)\boldsymbol{\varepsilon}(n) \tag{58}$$

The function $\min\{\boldsymbol{\varepsilon}^H\boldsymbol{\varepsilon}\}$ in (58) is expressed as the sum of two terms indicating that the backward parameters and forward parameters are uncorrelated and can be separately determined. The estimate of the forward parameters given in (32) therefore remains unchanged. The estimate of the backward parameters is given below as (following a similar mathematical manipulation),

$$\mathbf{A}_b = \begin{bmatrix} \mathbf{A}_b(0) \\ \text{------} \\ \mathbf{A}_b(1) \\ \vdots \\ \mathbf{A}_b(p) \end{bmatrix} = \begin{bmatrix} \mathbf{I}_N \\ \text{-------} \\ -\mathbf{R}_{bb}^{-1}\mathbf{R}_{b0} \end{bmatrix} \tag{59}$$

where $\mathbf{R}_{bb} \in \mathbb{C}^{pN \times pN}$ and $\mathbf{R}_{b0} \in \mathbb{C}^{pN \times N}$ are sub-block matrices of $\mathbf{R}_b \in \mathbb{C}^{(p+1)N \times (p+1)N}$ given as,

$$\mathbf{R}_b = \left[\begin{array}{c|c} \mathbf{R}_{00} & \mathbf{R}_{0b} \\ \hline \mathbf{R}_{b0} & \mathbf{R}_{bb} \end{array}\right] = \sum_{k=0}^{p-1} \mathbf{R}_u(k:k+p) \tag{60}$$

It is worth noting that the order of $\mathbf{A}_b$ in (59) is from low to high, contrary to the order of $\mathbf{A}_f$ in (32) which is from high to low. Also the divisions of the sub-block matrices in (33) and (60) used for computing $\mathbf{A}_f$ and $\mathbf{A}_b$, respectively, are different.

The manipulation matrix $\mathbf{B}$ given in (20) should be modified accordingly to include the backward prediction as,

$$\mathbf{B} = \left[\begin{array}{ccccccc} \mathbf{I}_N & \cdots & \mathbf{A}_b^H(p) & & & & \\ & \mathbf{I}_N & \cdots & \mathbf{A}_b^H(p) & & & \\ & & \ddots & & & & \\ & & & \mathbf{I}_N & \cdots & \mathbf{A}_b^H(p) & \\ \hline \mathbf{A}_f^H(p) & \cdots & \mathbf{I}_N & & & & \\ & \mathbf{A}_f^H(p) & \cdots & \mathbf{I}_N & & & \\ & & & \ddots & & & \\ & & & & \mathbf{A}_f^H(p) & \cdots & \mathbf{I}_N \end{array}\right] \tag{61}$$

Similarly the corresponding mean temporal residual covariance matrix is given as,

$$\overline{\mathbf{R}}_{\varepsilon} = \left[\begin{array}{c|c} \mathbf{I}_p \otimes \overline{\mathbf{R}}_{b\varepsilon} & \\ \hline & \mathbf{I}_{M-p} \otimes \overline{\mathbf{R}}_{f\varepsilon} \end{array}\right] \tag{62}$$

where

$$\overline{\mathbf{R}}_{b\varepsilon} = \frac{1}{p} \sum_{n=0}^{p-1} \mathbf{R}_{\varepsilon}(n) = \frac{1}{p} \mathbf{A}_b^H \mathbf{R}_b \mathbf{A}_b \tag{63}$$

Aimed at avoiding the dimensionality loss problem we have modified the PAMF algorithm using both the forward and backward predictions to maintain the dimensionality of the time sequence. The above formulation uses p points of

backward prediction and $M-p$ points of forward prediction. Obviously we can form other combinations if desired. We could select a combination containing a maximum number of points including $M-p$ points of backward prediction and $M-p$ points of forward prediction, for instance. However, according to the linear algebra, the maximum number of independent vectors after a linear transform is no greater than the original number of the independent vectors. Therefore, we do not expect that there would exist a combination which contains more independent vectors than the original.

To view the impact on the Doppler resolution and the processing gain due to the dimensionality reduction of PAMF, the example shown in Figure 4 is re-examined. To clearly show the impact we have chosen $M=10$ and $p=5$. The results are shown in Figure 32. The Doppler resolution of PAMF with forward prediction for this example is only a half of the Doppler resolution of the conventional STAP, since the PAMF process loses 50% of the time sequence. On the other hand we see the resolution of the PAMF with both backward and forward predictions is the same as that of the STAP, because of no dimensionality loss of the algorithm. A 3dB loss in the signal peak level for the process of the PAMF with forward prediction only is also observed.

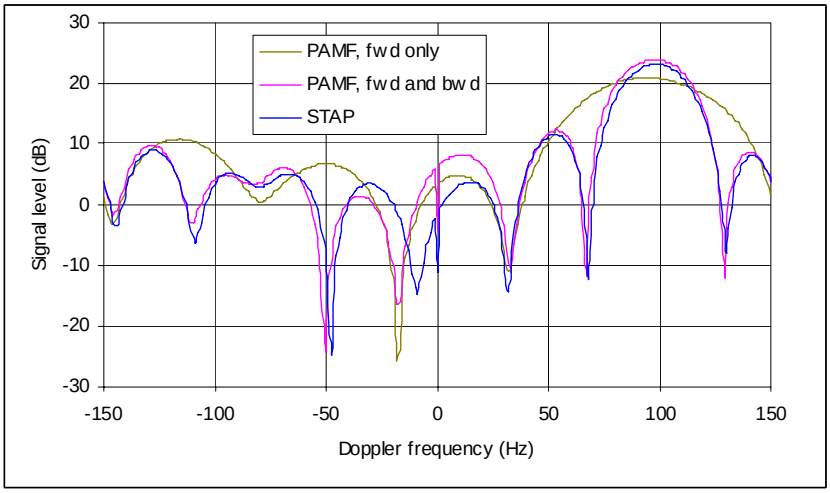

Figure 32: Doppler resolution comparison between the PAMF with forward prediction and the PAMF with both backward and forward predictions. The STAP result is also shown as a benchmark.

As the ratio of $(M-p)/M$ increases, the impact of the dimensionality loss fades. The detection results for target 1 in the RLSTAP dataset is plotted in Figure 33. In this example the values of $M=31$ and $p=5$ result in a 16% decrease in the Doppler resolution if the PAMF with forward prediction is used.

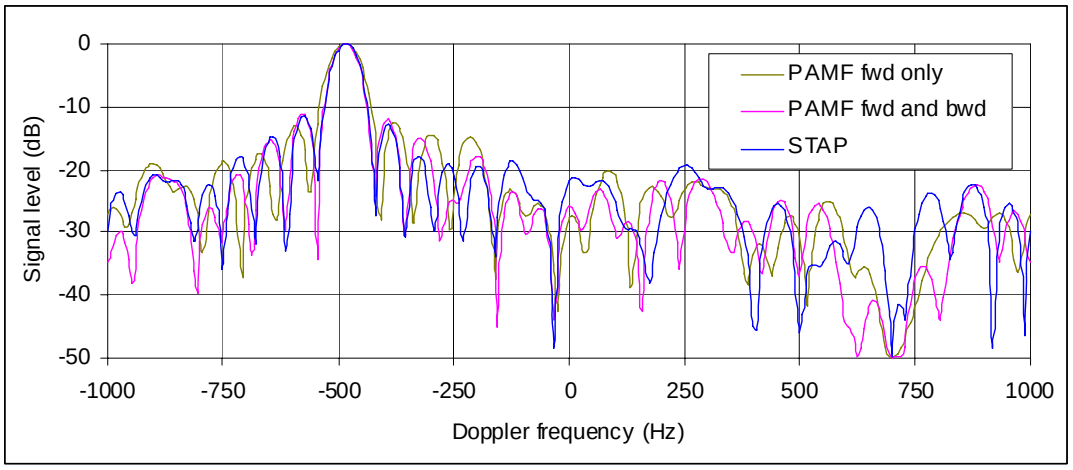

Figure 33: The impact of the dimensionality loss on the Doppler resolution and processing gain fades as the ratio of $(M-p)/M$ *increases. Shown is the target detection of target 1 in the RLSTAP dataset with* $M=31$ *and* $p=5$.

8. Summary

Much research effort, notably that carried out and sponsored by AFRL, has been made in developing and evaluating the PAMF approach for the last decade. This report has traced, analysed and evaluated this technique in great detail. Accessible publications of PAMF often omit details of the mathematics due to space limitation, making the papers difficult to follow. This report therefore has independently provided full mathematical derivation for a full understanding of the algorithm. The performance of the approach has then been assessed using three different types of data, namely data generated using a simple generic radar model, data generated by high fidelity radar simulation software, RLSTAP, and real radar data collected by the MCARM system. In the assessment, the results of the conventional space-time MF process have been used as benchmarks for comparison. The ops for the approach have also been estimated and computational savings of PAMF in comparison to the MF algorithm have been given. Finally a modification to the PAMF approach is proposed. The modified PAMF uses both the forward and backward prediction parameters to maintain the dimensionality of the process, so that the Doppler resolution and processing gain is maintained.

Based on the study, the PAMF algorithm has two advantages over the conventional MF algorithm:

- The ops requirement is less. Computational savings, compared to the MF algorithm, vary from less than 20% for a system with a small number of pulses

M and a small number of channels N, and a large number of range bins K_{rg}, to more than 90% for a system with large M and N, and small K_{rg}.

- The PAMF algorithm is much more robust than the MF algorithm in the case where the set of sample data is small.

Problems of the PAMF process include

- If PAMF uses the forward prediction parameters only, the equivalent temporal independent measurements are reduced from M to $M-p$ (p is the order of the filter, and M is the number of pulses in a CPI), which in turn reduces the Doppler resolution and the processing gain. The impact can be significant if the ratio of $(M-p)/M$ is small. However, as proposed, if PAMF is formed using both the forward and backward prediction, there is not a loss in dimensionality.
- The output of the PAMF MDTS processing does not seem to follow the pattern of the original clutter profile whereas the MF MDTS does (see Figure 23 and Figure 21). Whether this imposes a problem to target detection warrants a further investigation.

All simulations have suggested that using the sliding widow architecture to sample the covariance matrix for each range bin does not statistically improve results. Therefore a preferable option is to use the fixed window architecture to sample the covariance matrix and process a block of range bins, which significantly saves computational cost.

Overall the amount of ops required for the PAMF algorithm is still huge considering the time frame available for airborne radars. How to further reduce ops demand in processing phased array data warrants future research.

9. Acknowledgement

The Rome Laboratory, Air Force Material Command supplied the MCARM data and the RLSTAP software. Mr A Mahoney generated the RLSTAP data. Comments of Drs P Berry and J Whitrow in the vetting process are also acknowledged.

10. References

Brennan, L E, and Staudaher, F M, “Subclutter visibility demonstration”, Technical Report, RL-TR-92-21, Adaptive Sensors Incorporated, March 1992.

Bresler, Y, “Maximum likelihood estimation of a linearly structured covariance with application to antenna array processing”, *Proceedings of the Fourth Annual ASSP Workshop on Spectrum Estimation and Modelling*, pp. 172-175, 3-5 Aug 1988.

Carlson, B D, “Covariance matrix estimation erroes and diagonally loading in adaptive arrays,” *IEEE Trans on Aerospace and Electronic Systems*, vol. 24, no. 4, pp. 397-401, 1988.

Compton, Jr, R T, *Adaptive antennas, concepts and performance*, Prentice Hall, 1988.

Dong, Y, “Approximate invariance of the inverse of the covariance matrix and the resultant pre-built STAP processor”, Research Report, DSTO-RR-0291, DSTO, 2005.

Fenner, D, and Hoover, W F, “Test results of a space-time adaptive processing system for airborne early warning radar”, *Proceedings of IEEE 1996 National Radar Conference*, Ann Arbor, Michigan, 13-16 May 1996.

Gerlach, K, and Picciolo, M L, “Airborne/spacebased radar STAP using a structured covariance matrix”, *IEEE Trans on Aerospace and Electronic Systems*, vol. 39, no. 1, pp. 269-281, 2003.

Isaacson, E, and Keller, H B, *Analysis of Numerical Methods*, John Willey & Sons, Inc, 1966.

Klemm, R K, *Principles of space-time adaptive processing*, 2nd edn, IEE, 2002.

Marple, Jr, S L, *Digital Spectral Analysis with Applications*, Prentice-Hall Inc, 1987.

Michels, J R, Roman, J R, and Himed, B, “Beam control using the parametric adaptive matched filter STAP approach”, *Proceedings of IEEE Radar Conference 2003*, pp. 405-412.

MITRE, “STAP processing monostatic and bistatic MCARM data”, Final report prepared by MITRE, Centre for Air Force C2 Systems, Bedford, MA, 1999.

RAFDCI, “MCARM/STAP data analysis”, Final report, Part I and II, prepared by Research Associates for Defence Conversion Inc., New York, 1999.

Rangaswamy, M, and Michels, J H, “A parametric multichannel detection algorithm for correlated non-Gaussian random processes”, *Proceedings of 1977 IEEE National Radar Conference*, pp. 349-354, Syracuse, NY, 13-15 May.

Rangaswamy, M, Michels, J H, and Weiner, D D, “Multichannel detection for correlated non-Gaussian random processes based on innovations”, *IEEE Trans on Signal Processing*, vol. 43, no. 8, pp. 1915-1922, 1995.

Reed, I S, Mallett, J D, and Brennan, L E, “Rapid convergence rate in adaptive arrays”, *IEEE Trans on Aerospace and Electronic Systems*, vol. AES-10, no. 6, 1974.

Robey, F C, Fuhrmann, D R, Kelly, E J, and Nitzberg R, "A CFAR adaptive matched filter detector", *IEEE Trans on Aerospace and Electronic Systems*, vol. 28, no. 1, pp. 208-216, 1992.

Roman, J R, Davis, D W, and Michels, J H, "Multichannel parametric models for airborne phased array clutter", *Proceedings of 1977 IEEE National Radar Conference*, pp. 72-77, Syracuse, NY, 13-15 May.

Roman, J R, Rangaswamy, M, Davis, D W, Zhang, Q, Himed, B, and Michels, J H, "Parametric adaptive matched filter for airborne radar applications", *IEEE Trans on Aerospace and Electronic Systems*, vol. 36, no. 2, pp. 677-692, April 2000.

Sarkar, T K, Wang, H, Park, S, Adve, R, Koh, J, Kim, K, Zhang, Y, Wicks, M C, and Brown, R D, "A deterministic least-squares approach to space-time adaptive processing", *IEEE Trans on Antennas and Propagation*, vol. 49, no. 1, January 2001.

Sloper, D, Fenner, D, Arntz, J, and Fogle, E, "Multi-channel airborne radar measurement (MCARM), MCARM flight test", Westinghouse Electronic Systems, Final Technical Report, RL-TR-96-49, vol. 1, April 1996.

Steiner, M, and Gerlach, K, "Fast converging adaptive processor or a structured covariance matrix", *IEEE Trans on Aerospace and Electronic Systems*, vol. 36, no. 4, pp. 1115-1126, 2000.

Steiner, M, and Gerlach, K, "Fast converging maximum-likelihood interference cancellation," *Proceedings of IEEE 1998 National Radar Conference*, pp. 117-122, Dallas, TX, 12-13 May 1998.

Van Trees, H L, Optimum *Array Processing, Part IV, of Detection, Estimation and Modulation Theory*, Wiley Interscience, 2002.

Wang, H, and Cai, L, "On adaptive spatial-temporal processing for airborne surveillance radar systems", *IEEE Trans on Aerospace and Electronic Systems*, vol. 30, no. 3, pp. 660-670, 1994.

Wang, Y L, Chen, J W, Bao, Z, and Peng, Y N, "Robust space-time adaptive processing for airborne radar in nonhomogeneous clutter environments", *IEEE Trans on Aerospace and Electronic Systems*, vol. 39, no. 1, pp. 70-81, 2003.

Ward, J, "Space-time adaptive processing for airborne radar", Technical Report TR-1015, Lincoln Laboratory, MIT, 1994.

Ward, J, and Kogon, S M, "Space-time adaptive processing (STAP) for AMTI and GMTI radar", tutorial slides, CD of the *Proceedings of 2004 IEEE Radar Conference*, Philadelphia Pennsylvania, 26-29 April 2004.

Parametric Adaptive Matched Filter and its Modified Version

Yunhan Dong

(DSTO-RR-0313)

AUSTRALIA

DEFENCE ORGANISATION	**No. of copies**
Task Sponsor, DCEO-DMO	1 printed
S&T Program	
Chief Defence Scientist	1
Deputy Chief Defence Scientist Policy	1
AS Science Corporate Management	1
Director General Science Policy Development	1
Counsellor Defence Science, London	Doc Data Sheet
Counsellor Defence Science, Washington	Doc Data Sheet
Scientific Adviser to MRDC, Thailand	Doc Data Sheet
Scientific Adviser Joint	1
Navy Scientific Adviser	1
Scientific Adviser – Army	1
AirForce Scientific Adviser	1
Scientific Adviser to the DMO	1
Platforms Sciences Laboratory	
Deputy Chief Defence Scientist Aerospace	Doc Data Sht & Exec Summ
Systems Sciences Laboratory	
EWSTIS (soft copy for accession to EWSTIS Web site)	1
Chief, Electronic Warfare and Radar Division	Doc Data Sht & Dist List
Research Leader, Maritime EW	Doc Data Sht & Dist List
Research Leader, Air EW	Doc Data Sht & Dist List
Research Leader, JIL EW	Doc Data Sht & Dist List
Research Leader, Microwave Radar	Doc Data Sht & Dist List
Head, ES Systems	Doc Data Sheet
Head, RF Countermeasures	Doc Data Sheet
Head, RF Technology	Doc Data Sheet
Head, Strategic and Land EW	Doc Data Sheet
Head, Aerospace Systems	Doc Data Sheet
Head, Maritime Systems	Doc Data Sheet
Head, EO Countermeasures	Doc Data Sheet
Head, EO Technology	Doc Data Sheet
Head, Radar Systems and Technologies	Doc Data Sheet
Head, Maritime Air Surface	Doc Data Sheet
Head, Maritime Surface Radar	Doc Data Sheet
Head, Radar Signatures	Doc Data Sheet

Task Manager: Scott Capon, EWRD	1 printed
Yunhan Dong, EWRD	1 printed
DSTO Library and Archives	
Library Edinburgh	1 printed + Doc Data Sheet
Defence Archives	1 printed
Library Canberra	Doc Data Sheet
Capability Development Group	
Director General Maritime Development	Doc Data Sheet
Director General Land Development	1
Director General Capability and Plans	Doc Data Sheet
Assistant Secretary Investment Analysis	Doc Data Sheet
Director Capability Plans and Programming	Doc Data Sheet
Director General Australian Defence Simulation Office	Doc Data Sheet
Chief Information Officer Group	
Director General Australian Defence Simulation Office	Doc Data Sheet
AS Information Strategy and Futures	Doc Data Sheet
Strategy Group	
Director General Military Strategy	Doc Data Sheet
Assistant Secretary Governance and Counter-Proliferation	Doc Data Sheet
Navy	
Maritime Operational Analysis Centre, Building 89/90 Garden Island Sydney NSW	Doc Data Sht & Dist List
Deputy Director (Operations)	
Deputy Director (Analysis)	
Director General Navy Capability, Performance and Plans, Navy Headquarters	Doc Data Sheet
Director General Navy Strategic Policy and Futures, Navy Headquarters	Doc Data Sheet
Air Force	
SO (Science) - Headquarters Air Combat Group, RAAF Base, Williamtown NSW 2314	Doc Data Sht & Exec Summ
Army	
ABCA National Standardisation Officer	e-mailed Doc Data Sheet
Land Warfare Development Sector, Puckapunyal	
SO (Science) - Land Headquarters (LHQ), Victoria Barracks NSW	Doc Data Sht & Exec Summ
SO (Science), Deployable Joint Force Headquarters (DJFHQ) (L), Enoggera QLD	Doc Data Sheet
Joint Operations Command	
Director General Joint Operations	Doc Data Sheet

Chief of Staff Headquarters Joint Operations Command	Doc Data Sheet
Commandant ADF Warfare Centre	Doc Data Sheet
Director General Strategic Logistics	Doc Data Sheet
COS Australian Defence College	Doc Data Sheet

Intelligence and Security Group

AS Concepts, Capability and Resources	1
DGSTA , DIO	1
Manager, Information Centre, Defence Intelligence Organisation	1

Defence Materiel Organisation

Deputy CEO	Doc Data Sheet
Head Aerospace Systems Division	Doc Data Sheet
Head Maritime Systems Division	Doc Data Sheet
Program Manager Air Warfare Destroyer	Doc Data Sheet

OTHER ORGANISATIONS

National Library of Australia	1
NASA (Canberra)	1

UNIVERSITIES AND COLLEGES

Australian Defence Force Academy	
Library	1
Head of Aerospace and Mechanical Engineering	1
Hargrave Library, Monash University	Doc Data Sheet

OUTSIDE AUSTRALIA

INTERNATIONAL DEFENCE INFORMATION CENTRES

US Defense Technical Information Center	1
UK Dstl Knowledge Services	1
Canada Defence Research Directorate R&D Knowledge & Information Management (DRDKIM)	1
NZ Defence Information Centre	1

ABSTRACTING AND INFORMATION ORGANISATIONS

Library, Chemical Abstracts Reference Service	1
Engineering Societies Library, US	1
Materials Information, Cambridge Scientific Abstracts, US	1
Documents Librarian, The Center for Research Libraries, US	1

INFORMATION EXCHANGE AGREEMENT PARTNERS

National Aerospace Laboratory, Japan	1
National Aerospace Laboratory, Netherlands	1

SPARES 5 printed

Total number of copies: 38 Printed: 10 PDF: 28

Page classification: UNCLASSIFIED

DEFENCE SCIENCE AND TECHNOLOGY ORGANISATION DOCUMENT CONTROL DATA				
				1. PRIVACY MARKING / CAVEAT (OF DOCUMENT)
2. TITLE Parametric Adaptive Matched Filter and its Modified Version			3. SECURITY CLASSIFICATION (FOR UNCLASSIFIED REPORTS THAT ARE LIMITED RELEASE USE (L) NEXT TO DOCUMENT CLASSIFICATION) Document (U) Title (U) Abstract (U)	
4. AUTHOR(S) Yunhan Dong			5. CORPORATE AUTHOR Defence Science and Technology Organisation PO Box 1500 Edinburgh SA 5111	
6a. DSTO NUMBER DSTO-RR-0313	6b. AR NUMBER AR-013-643		6c. TYPE OF REPORT Research Report	7. DOCUMENT DATE May 2006
8. FILE NUMBER 20006 / 1060092	9. TASK NUMBER AIR 05 / 264	10. TASK SPONSOR DCEO-DMO	11. NO. OF PAGES 70	12. NO. OF REFERENCES 38
13. URL on the World Wide Web http: / / www.dsto.defence.gov.au / corporate / reports / DSTO-RR-0313.pdf			14. RELEASE AUTHORITY Chief, Electronic Warfare and Radar Division	
15. SECONDARY RELEASE STATEMENT OF THIS DOCUMENT Approved for Public Release OVERSEAS ENQUIRIES OUTSIDE STATED LIMITATIONS SHOULD BE REFERRED TO DOCUMENT EXCHANGE, PO BOX 1500, EDINBURGH, SA 5111, AUSTRALIA				
16. DELIBERATE ANNOUNCEMENT No Limitations				
17. CASUAL ANNOUNCEMENT Yes				
18. DSTO RESEARCH LIBRARY THESAURUS Adaptive filters Airborne radar Space-time adaptive processing Mathematical analysis				

19. ABSTRACT

The parametric adaptive matched filter (PAMF) for space-time adaptive processing (STAP) has been an interesting research area in the airborne radar data processing community over the last decade. Starting from providing a complete formulation of PAMF, this report assesses the performance of PAMF using simulated data as well as real airborne data collected by the Multi-channel Airborne Radar Measurements (MCARM) system with use of results from the conventional STAP as a benchmark. A modified PAMF approach using both forward and backward predictions is proposed to eliminate the dimensionality loss of the method. Finally the operational counts and computational savings of PAMF are also estimated.